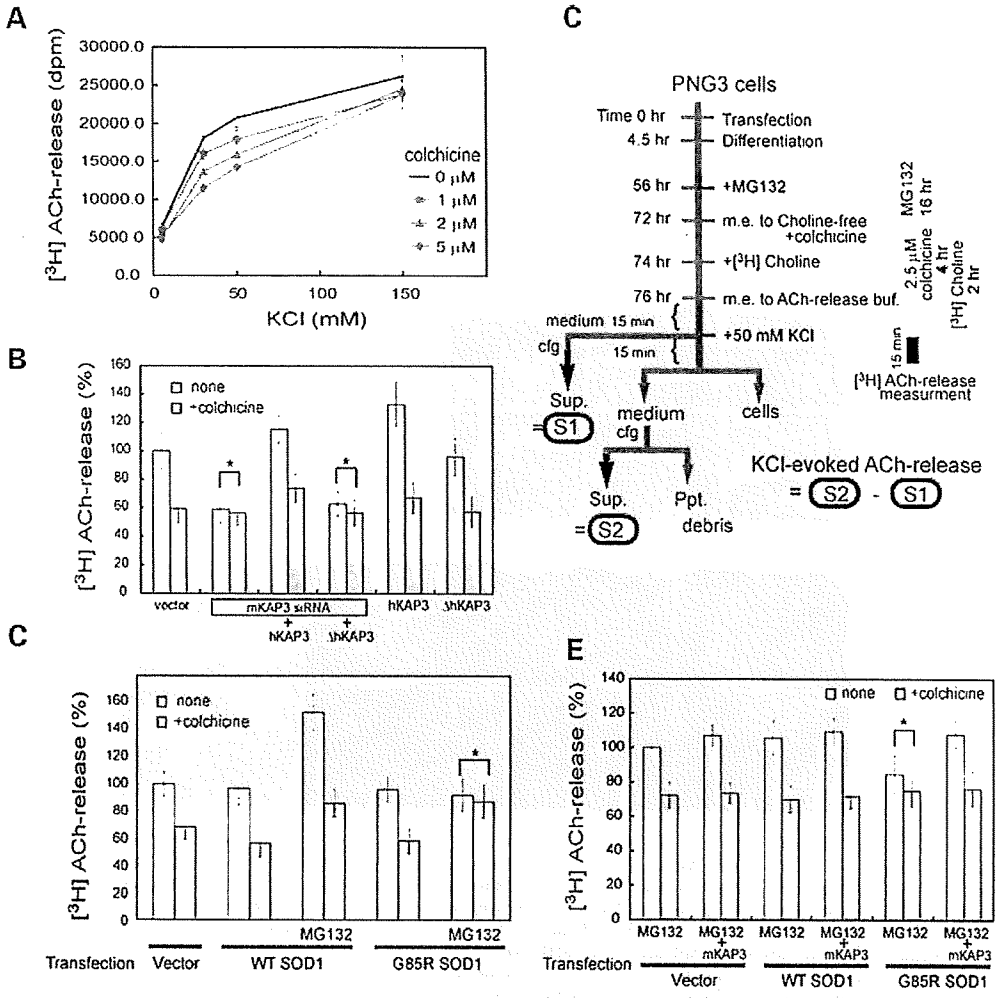


**Figure 6.** Microtubule-dependent fraction of depolarization-induced ACh release from PNG3 cells requires KAP3. (**A**) Differentiated PNG3 cells, metabolically labeled with [$^3$H]choline, were depolarized by increased KCl in the medium for 15 min. The radioactivity was released into the medium representing [$^3$H]ACh and was measured for different concentrations of KCl and colchicine, as indicated. (**B**) Depolarization-induced [$^3$H]ACh release from differentiated PNG3 cells transfected with vector only, siRNA for mouse KAP3 (mKAP3) or siRNA for mKAP3 together with expression plasmid for either human KAP3 (hKAP3) or hKAP3 lacking C-terminal 223 amino acids (ΔhKAP3), expression plasmid for hKAP3 only or expression plasmid for ΔhKAP3 was determined with or without colchicine treatment. Radioactivity is shown as a percentage to that from vector-transfected, colchicine-untreated cells. The asterisk indicates non-significant differences calculated as $P > 0.05$. Note that KAP3 down-regulation inhibited microtubule-dependent ACh release. (**C**) Summarized time schedule for [$^3$H]ACh-release measurement in differentiated PNG3 cells with and without SOD1 misfolding/aggregation. KCl-evoked release of ACh was calculated by subtracting the radioactivity in S1 (medium before KCl addition) from that in S2 (medium after KCl addition). (**D**) Depolarization-induced [$^3$H]ACh release from differentiated PNG3 cells transfected with vector only, expression plasmid for wild-type SOD1 or G85RSOD1 was determined with or without MG132 treatment. Microtubule-dependent and -independent fractions of release were measured for each condition analyzed. Radioactivity is shown as percentage to that from vector-transfected, colchicine-untreated cells. Note that ACh release from mutant SOD1-transfected cells was reduced in response to MG132 treatment, while overexpression of mutant SOD1 *per se* did not affect choline incorporation into cells (Supplementary Material, Fig. S4C). The asterisk indicates non-significant difference calculated as $P > 0.05$. (**E**) Depolarization-induced [$^3$H]ACh release from differentiated PNG3 cells transfected with vector only, expression plasmid for wild-type SOD1 or G85RSOD1, with or without co-transfection of mKAP3 expression plasmid, was determined after MG132 treatment. Microtubule-dependent and -independent fractions of release were measured for each condition analyzed. Radioactivity is shown as a percentage of that from vector-transfected, colchicine-untreated cells. Note that the reduction in ACh release observed in mutant SOD1-transfected cells in response to MG132 treatment was normalized by mKAP3 expression. The asterisk indicates non-significant difference calculated as $P > 0.05$.

(Fig. 6D, asterisk). MG132 treatment itself resulted in up-regulation of both microtubule-dependent and -independent ACh release (Fig. 6D and Supplementary Material, Fig. S4A). However, this MG132-induced increase in ACh release was presumably caused by increased expression levels of proteins necessary for ACh synthesis/release and was independent from the misfolded SOD1-induced effect (Supplementary Material, Figs S4B and C). These results suggest that misfolded SOD1 inhibits ChAT transport in this FALS model system in culture as well.

The observations in *SOD1*$^{G93A}$-Tg mice, as well as in the cellular FALS model system that we described, further

suggest that misfolded SOD1 causes a reduction or depletion of the functional kinesin-2 complex via its association with KAP3. This raises the possibility that misfolded SOD1-induced reduction in ChAT transport may be normalized by supplementing motor neurons with KAP3. To prove this hypothesis using the FALS culture model system, we examined microtubule-dependent ACh release from differentiated PNG3 cells overexpressing wild-type or mutant SOD1 together with KAP3. Overexpression of KAP3 did not change ACh release from MG132-treated PNG cells transfected with empty vector or wild-type SOD1. However, overexpression of KAP3 was able to normalize the ACh release reduction under the condition that causes mutant SOD1 misfolding (Fig. 6E). These results strongly suggest that misfolded SOD1-induced reduction in ChAT transport and ACh release is mediated by a reduction in functional KAP3 molecule because of its association with misfolded SOD1. These results may also suggest that the normalization of functional KAP3 level in motor neurons could have a therapeutic effect on FALS pathogenesis.

### KAP3 was co-localized with mutant SOD1 aggregates within LBHI in spinal motor neurons from human FALS patients

As described, we performed analysis of the misfolded SOD1-induced reduction of ChAT transport in cultured cells in cultured cells as well as in a mouse model. To gain insight into the significance of this mechanism in human FALS, we performed immunohistochemistry on spinal cord sections of human SOD1-linked FALS cases to examine co-localization of KAP3 and SOD1. The neuropathological phenotypes of four patients we analyzed, who were members of two different families (27–29), are summarized in a table in Figure 7. These patients often developed Lewy-body-like hyaline inclusions (LBHIs), which are protein aggregates containing mutant/wild-type SOD1 and one of the most characteristic cytopathological changes in the spinal motor neurons of mutant *sod1*-linked FALS (28). Immunohistochemical analysis revealed that most of the LBHIs in the spinal motor neurons were positive for both KAP3 and SOD1 (arrowheads in Fig. 7). We confirmed that the KAP3 signal in LBHIs was not present when the anti-KAP3 antibody was pre-incubated with an excess of the synthetic KAP3 antigen peptides (data not shown). These observations demonstrated that KAP3–SOD1 interaction and subsequent co-aggregation frequently occurs in human SOD1-linked FALS cases.

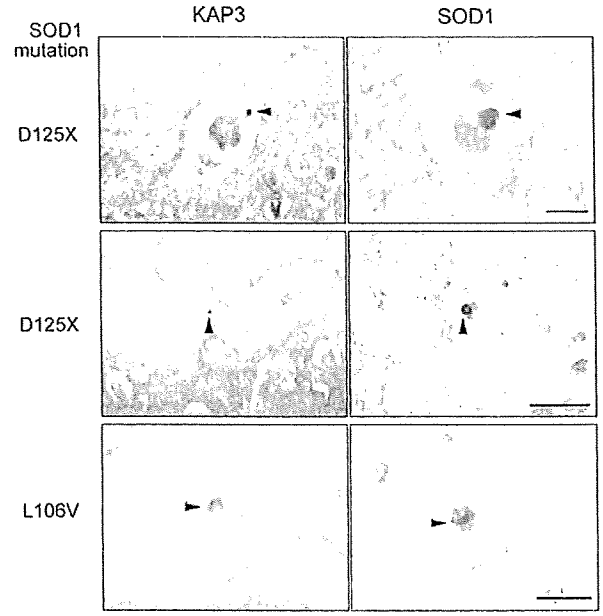


Neuropathological findings in autopsied patients with FALS examined.

| SOD1 mutation | Number of patients | Neuronal inclusion | SOD1 aggregation | Bunina body | Corticospinal tract involvement | Posterior column involvement |
|---|---|---|---|---|---|---|
| D125X | 2 | LBHI | + | - | + | + |
| L106V | 2 | LBHI | + | - | + | + |

+ present, - absent, LBHI: Lewy-body-like hyaline inclusion

**Figure 7.** KAP3 was co-localized with SOD1 aggregates within LBHI in spinal motor neurons from human FALS cases. Consecutive sections of LBHI-containing spinal motor neurons from FALS patients possessing *sod1* mutations were immunostained with anti-KAP3 and anti-SOD1 antibodies. The clinicopathological characteristics of the FALS patients are summarized in the table. D125X mutation is a deletion of two nucleotides at codon 126 that results in the truncation of five residues downstream. Co-localization of KAP3 and SOD1 within the LBHI is evident (arrowheads). The images are representative of 30 LBHIs observed in each case, all of which showed co-localization of SOD1 and KAP3. Scale bars=25 μm for the images of top row, 50 μm in others.

## DISCUSSION

In this paper, we presented a novel pathological mechanism by which misfolded SOD1 may cause neuronal dysfunction in FALS. A significant proportion of misfolded SOD1 is located within motor axons prior to disease onset in *SOD1*$^{G93A}$-Tg FALS model mice. We showed that misfolded SOD1 species selectively binds to KAP3 (Fig. 2B and C) and that this binding may be a cause for the reduction in functional KAP3 molecule required for kinesin-2-dependent transport within motor axons (Fig. 3A and B). The kinesin-2 motor complex is particularly important, because it is required for ChAT transport (19). Decreased ChAT expression and resultant decrease in ACh release from motor nerve ends can lead to dysfunction of motor synapses at axon terminals (30,31). By employing a newly developed cell culture model of FALS, we showed that ACh release from nerve terminals was decreased presumably due to a reduction in ChAT transport resulting from KAP3 sequestration by misfolded SOD1 species (Figs 5A and C and 6D). The pathological mechanism we propose from our data is schematized in Figure 8.

ALS-like motor neuron pathology is observed in transgenic mice expressing C-terminal truncated SOD1 (L126Z), in which the mutant SOD1 expression was not clearly observed in sciatic nerve (32). This suggests that KAP3-misfolded SOD1 association is formed mostly in motor neuron cell bodies. Indeed, we detected KAP3-misfolded SOD1 associ-

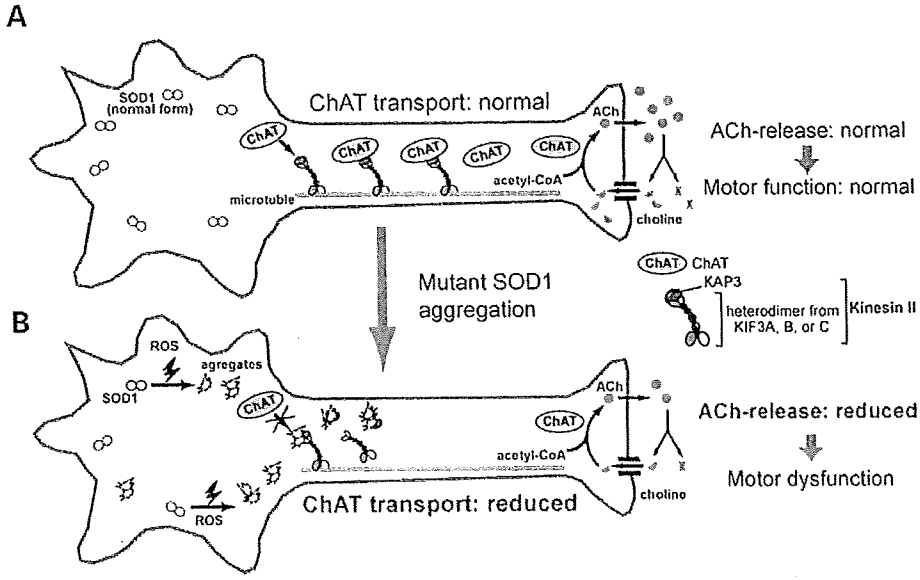


**Figure 8.** A schematic diagram for a mutant SOD1 toxicity and impairment of axonal transport of ChAT. In healthy motor neurons (**A**), ChAT is continuously transported by kinesin-2 motor, comprising KIF3A, KIF3B/C and KAP3, toward the neuromuscular junction where ACh functions as a neurotransmitter. ACh is released into the synaptic cleft upon stimulation and rapidly degraded into choline and acetic acid by AChE. Choline is taken up into the nerve terminal by choline transporters and then ChAT synthesizes ACh from choline and acetyl-CoA. The reaction catalized by ChAT is the rate-limiting step for ACh supply to the nerve terminals. In motor neurons expressing mutant SOD1 (**B**), mutant SOD1 proteins were converted into misfolded forms as a result of increased ROS generation and/or reduced proteasomal activity. Certain misfolded species preferentially binds to KAP3 and inhibit the binding of ChAT to KAP3, thereby causing a decrease in ChAT transport. This decrease in ChAT in the nerve terminals can constitute a mechanism that causes motor dysfunction.

ation in spinal cords (Fig. 2C) and ventral white matter (Fig. 2A and B) of *SOD1*$^{G93A}$-Tg mice prior to disease onset, but could not detect it in distal sciatic nerve even at the end-stage (data not shown). These findings suggest that, even if misfolded SOD1 associates with molecular motors, it cannot travel for a long distance, presumably because it is not a physiological cargo.

We suspect that misfolded SOD1–KAP3 association is one of the early events in FALS pathogenesis. Evidence to support this possibility is that the SOD1–KAP3 association becomes detectable around 6 months of age in *SOD1*$^{G93A}$-Tg mice, 2 months earlier than disease onset (Fig. 2C), suggesting that the SOD1–KAP3 association constitutes an early event in FALS motor neurons. Also, our immunoprecipitation/immunoblot analysis shows that SOD1–KAP3 association always detected relatively low molecular-weight misfolded SOD1 (−50 kDa) among all of the misfolded products ranging up to hundreds of kilodaltons in size (Figs 2B and C and 5A). The preferential association of KAP3 for low molecular-weight species but not with large precipitates suggests that SOD1–KAP3 association accounts for a fraction of the initial events in FALS pathogenesis. Previous reports on selective increase in KAP3 transcription in lumbar spinal cords from *SOD1*$^{G86R}$-Tg mice as an early event prior to disease onset (33) also supports our hypothesis, as the increase may be regarded as compensatory to the KAP3 sequestration by SOD1–KAP3 association.

Previous reports show that crossing mutant SOD1-Tg mice with dynein heavy chain mutant mice (*loa* or *cra*) delays the disease onset and extends survival (34,35). This result is surprising because mutations in dynein heavy chain, a subunit of dynein motor complex, or p150$^{Glued}$, a subunit of dynactin (dynein activator) cause dysfunction and degeneration of spinal motor neurons (15,16). This suggests a possible mechanistic link between impaired axonal transport in mutant *SOD1*-Tg mice and that in dynein heavy chain mutant mice. Here we demonstrated that KAP3 sequestration by misfolded SOD1 is a mechanism for selective inhibition of axonal transport observed in mutant SOD1-Tg mice. Previous reports on melanophore transport in *Xenopus* melanosomes showed that dynactin serves as an activator of kinesin-2 via direct binding of p150$^{Glued}$ to KAP3 and regulates the intracellular direction of melanosome transport by binding to either dynein (retrograde) or KAP3 (anterograde) (36). Dynein and KAP3 share the same binding site on p150$^{Glued}$, and so p150$^{Glued}$ binds to only one of them at a time and thereby activates transport in only one direction. If a similar regulation by dynactin plays a role in mammalian neurons, *loa* and *cra* mutations may increase the chance of p150$^{Glued}$ to bind to KAP3, because those mutations promote subunit disassembly and increase dynein-unbound dynactin (15). By this mechanism, dynein heavy chain mutations may result in normalizing kinesin-2-mediated transport of ChAT inhibited by the misfolded SOD1 species. Indeed, in our analysis of ventral white matter in *SOD1*$^{G93A}$-Tg mice using Nycodenz density gradient centrifugation, a small fraction of p150$^{Glued}$ co-migrated with misfolded SOD1 species and KAP3 (Fig. 2A). This population of p150$^{Glued}$ also co-precipitated with KAP3 (data not shown). This result may reflect an involvement of p150$^{Glued}$ in KAP3/SOD1 misfolding and aggregation through its interaction with KAP3.

A recent study provides an interesting evidence that transcription of all members of the KIF3 family selectively decreases in motor cortex of sporadic ALS patients among 13 kinds of kinesin and kinesin-related proteins (37). Impaired neuromuscular transmission was detected in early sporadic ALS patients (38), and a reduced supply of releasable ACh was thought to be the primary cause for the degeneration of motor terminal in a dog model of hereditary spinal muscular atrophy (30,39). It is possible that kinesin-2 dysfunction and subsequent inhibition of ChAT transport might be one of the common pathways leading to motor neuron-specific dysfunction in both sporadic and familial ALS cases.

The cargos and adaptor molecules for kinesin-2 have not been well studied. Small GTP-binding protein dissociation factor SmgGDS (40), fodrin (41), a tumor suppressor adenomatous polyposis coli (42), N-cadherin (43), ChAT and AChE (18) have been reported as molecules that bind to KAP3. Our finding that misfolded SOD1 species sequesters KAP3 raises a possibility that the transport of these molecules may also be impaired in mutant SOD1-related FALS, together with the reduced ChAT transport. Indeed, we observed a slight decrease in N-cadherin transport in motor axons from presymptomatic *SOD1*$^{G93A}$-Tg mice (Supplementary Material, Fig. S5). The expression and function of those molecules within motor neurons need to be studied to elucidate the entire mechanism.

## MATERIALS AND METHODS

All the data in Figures 1–6 are a representative of three mice per group or three independent experiments. Statistical significance was assessed by ANOVA followed by Fisher's test. Error bars in graphs represent standard deviations. Signals in immunoblots were detected using ECL (GE Healthcare) and quantified with NIH image software (1.61J).

### Reagents

All four types (WT, G93A, G85R and A4V) of FLAG-tagged human SOD1 cDNA at the C terminus were cloned into pcDNA3 (44). Full-length mouse (Image clone ID: 5698182) and human (4829354) KAP3 were purchased from Image clone bank and cloned into pcDNA3 and pCMV-Tag1, respectively. The integrity of each clone was verified by nucleotide sequence analysis. The siRNA designed for silencing mouse KAP3 (M-047278-00-0010) was purchased from Dharmacon Research. Primary antibodies used for immunoblots were as follows: anti-SOD1 (Stressgen, SOD-100, and Calbiochem, 574597), kinesin C2 (Affinity BioReagents) and CRMP-2 (Immuno-Biological Laboratories). Anti-ChAT (AB144P), KHC (MAB1614), KLC (MAB1617), synaptophysin (MAB5258-20UG), actin (MAB1501), Neurofilament-M (AB1987) and MBP (myelin basic protein, AB9046) antibodies were all purchased from Chemicon. Anti-KAP3, KIF3A, KIF3B, p150$^{Glued}$, p50 dynamitin, dynein IC, KIF2 and Rab3 antibodies were purchased from BD PharMingen/Transduction Laboratories. Primary antibodies used for immunoprecipitation and immunostaining were anti-SOD1 (Stressgen, SOD-100), ChAT (Chemicon, AB144P) and FLAG (Sigma, F3165) antibodies. KAP3 antibody was prepared by immunizing rabbits with a peptide containing the 1–14 amino acids of mouse KAP3, which are conserved in human KAP3, followed by affinity purification using an epitope-conjugated column.

### Animals

We used the G1L line of transgenic mice harboring the G93A-mutated human *SOD1* gene (B6SJL-*TgN*(*SOD1-G93A*)1Gur$^{dl}$) purchased from the Jackson Laboratories. Mice harboring wild-type human *SOD1* gene (B6.Cg-*Tg*(*SOD1*)2Gur/J) was a gift from Dr Kawamata of Kyoto University. C57BL/6J mice were also used. The transgenic mice were backcrossed with C57BL/6J for more than 14 generations. All data were derived from male mice. All the animal experiments were approved by the Animal Care Committee of National Center of Neurology and Psychiatry (NCNP).

### Preparation of subsegments from mouse spinal cords using LMD technique

Frozen sections from mouse spinal cords were prepared without fixation and processed through AS LMD (Leica) as previously described (17). Five sections were pooled for each sample location for subsequent analyses.

### Isolation of misfolded SOD1 species from ventral white matter of spinal cords

The spinal cord was dissected from the indicated mice, and the ventral half of white matter at L1-S3 level was carefully dissected under a microscope. The dissected samples were homogenized in 300 μl of Nz homogenization buffer [20 mM HEPES, pH 7.4, 120 mM NaCl, 2 mM EDTA, pH 8.0, 0.25% NP-40 and complete protease inhibitor cocktail (Roche)] followed by a brief sonication., The lysates were added to 3.2 ml of Nycodenz linear density gradient in 10 mM HEPES, pH 7.4 and 1 mM EDTA, pH 8.0 (initial concentration of Nycodenz was 30%). After a centrifugation at 87 479*g* for 2 h at 4°C, in Optima MAX-E using MLS 50 rotor (Beckman Coulter), 160 μl of aliquot was collected from the top to the bottom of the tube, totaling 22 fractions. Twenty microliters of each fraction was collected and analyzed by immunoblot.

### Immunoprecipitation

Affinity-purified anti-KAP3 and anti-SOD1 antibodies were captured with Dynabeads Protein G (Dynal Biotech) and cross-linked using dimethyl pimelimidate as per manufacturer's protocol. For the immunoprecipitation from fractions prepared from Nycodenz density gradient centrifugation, 30 μl of each fraction was mixed with the antibody-conjugated Dynabeads in 20 mM HEPES, pH 7.4, 120 mM NaCl, 2 mM EDTA and complete protease inhibitor cocktail. The mixture was incubated overnight at 4°C on a rocking platform, followed by washing with PBS containing 0.05% Tween-20. The target proteins were eluted with 30 μl of 0.1 M citric acid (pH 2.0) for 2 min, and half of the eluates

were analyzed. For the immunoprecipitation from spinal cords or SOD1-transfected PNG3 cells, tissues or cells were lysed in TN-T buffer (50 mM Tris–HCl, pH 7.6, 1% Triton X-100, 150 mM NaCl) containing complete protease inhibitor cocktail and subjected to a centrifugation at 5000*g* for 10 min at 4°C. The supernatants were incubated with antibody-conjugated Protein G Dynabeads and analyzed as described above.

### Preparation of transported components from ventral cauda equina

The fraction enriched with transported components within motor axons was prepared from ventral roots of caudal spinal cords as described (41) with the following modifications. Ventral cauda equina was minced for two times in 400 μl of IM-D buffer supplemented with 1 mM ATP and a protease inhibitor cocktail (Complete; Roche) for 10 min on ice. They were subsequently subjected to centrifugation at 5000*g* for 10 min at 4°C. The obtained supernatants were measured for protein concentration and 5 μg of each was subjected to SDS/PAGE to evaluate the kinesin-2 contents. To analyze kinesin-2 status, the transported vesicle fractions prepared from four mice were subjected to 4.4 ml of sucrose step gradient centrifugation ranging from 0.2 to 2%. After centrifugation in an SW55 Ti rotor (Beckman Coulter) at 50 000 rpm for 18 h at 4°C, 400 μl of each fraction was collected from top of the tube, totaling 12 fractions, and 20 μl of each fraction was analyzed by SDS–PAGE/immunoblots.

### Cell culture and transfection

NG108-15 cells (a kind gift from Dr Akazawa in Tokyo Medical and Dental University), a hybrid cell line of mouse N18TG2 neuroblastoma cells and rat C6-BU-1 glioma cells, were cultured in Dulbecco's modified Eagle's medium (DMEM) (Sigma, D5796) containing 10% fetal bovine serum and 2% HAT supplement (GIBCO). Differentiation of PNG3, a subclone of NG108-15 isolated from single cells, was induced with 1 mM of dibutyryl cAMP (Nacalai tesque) and 0.2 μM of dexamethasone (MB Biomedicals) for 3 days. Transfection of plasmids into PNG3 was performed using Optifect or Lipofectamine 2000 (Invitrogen Life Technologies) as per manufacturer's protocol. Culture medium was changed every 20–24 h except where indicated otherwise. Transfection of siRNA and co-transfection of siRNA with plasmids were performed according to the manufacturer's protocols using DharmaFECT transfection reagent 2 (Dharmacon) and DharmaEFCT Duo transfection reagent, respectively. For induction of SOD1 misfolding/aggregation, cells were treated with 6.5 μM of MG132 (a proteasome inhibitor) 56 h after transfection and then treated with 2.5 mM hydrogen peroxide for 2 h at 72 h after transfection. Cells were then lysed with TN-T buffer plus Complete protease inhibitor cocktail and subjected to centrifugation at 10 000*g* for 10 min at 4°C to be separated into soluble (supernatant) and insoluble (pellet) fractions.

### Measurement of [$^3$H]ACh release

Depolarization-induced [$^3$H]ACh release was measured based on the method previously described (Kumagai *et al.*, 1993) with several modifications. For metabolic labeling of PNG3 cells by [$^3$H]choline, DMEM lacking choline chloride was used. Time schedules for labeling, reagents used and incubation time are shown in Figure 6C.

The culture medium was changed to choline-free DMEM either with or without colchicine. After 2 h incubation, 6.25 kBq [$^3$H]choline chloride ([methyl-$^3$H] choline chloride, 2.2 TBq/mmol; GE Healthcare) was added to the medium of each well of a 12-well plate. After 2 h incubation, the medium was changed to ACh release measuring buffer [20 mM HEPES-NaOH, pH 7.4, 150 mM NaCl, 5 mM KCl, 1.8 mM $CaCl_2$, 0.8 mM $MgSO_4$, 25 mM glucose, 25 μM eserine sulfate and 10 μM hemicholinium-3 (HC-3)] and the culture plates were returned to the $CO_2$ incubator. Eserine, an inhibitor for cholinesterase, was added to inhibit a degradation of released ACh by cholinesterase. HC-3, an inhibitor for high-affinity choline transporter 1, was added to completely inhibit [$^3$H]choline uptake after changing the medium. After 15 min incubation, with eserine and HC-3, an aliquot of culture medium was transferred into a 1.5 ml tube (media before KCl addition), and then KCl was added into the medium to a final concentration of 50 mM. The culture plates were quickly returned to the $CO_2$ incubator, and after 15 min, the medium was transferred into a new 1.5 ml tube (media after KCl addition). Both the medium collected before and after KCl addition were centrifuged at 10 000*g* for 5 min at 4°C to remove debris. The supernatants were mixed with a scintillation cocktail (Ultima Gold XR, Perkin Elmer) to measure the [$^3$H] radioactivity using a liquid scintillation spectrophotometer. The radioactivity of [$^3$H]ACh released by KCl was calculated by subtracting the activity of media before KCl (=S1) from the activity of media after KCl addition (=S2), as described in Figure 6C.

### Immunocytochemistry

PNG3 cells were fixed with 4% paraformaldehyde in PBS for 15 min. After permeabilization with 0.15% Triton X-100 in PBS for 10 min, cells were treated with Blocking-one (Nacalai) for 1 h. The cells were then treated with primary antibodies in Blocking-one at 4°C overnight. The cells were washed with PBS. For detection, cells were treated with fluorescent-conjugated secondary antibodies in Blocking-one at room temperature for 1 h. After washing again with PBS, cells were mounted with Vectasheld (Vector Laboratories).

### Autopsy specimens and immunohistochemistry

The studies were performed on archival, buffered 10% formalin-fixed, paraffin-embedded spinal cord tissues obtained at autopsy from four FALS patients who were members of two different families. Consent for autopsy was obtained from legal representatives in accordance with the requirements of local institutional review boards. The clinicopathological characteristics of the FALS patients have been previously reported (27,29). SOD1 gene analysis revealed that the members of the Japanese Oki family had a 2 bp deletion at codon 126 in the gene for SOD1 (frame-shift 126 mutation, D125X) and that the members of the T family had a Leucine to Valine substitution at codon 106 in the SOD1

gene (L106V). To look at the expression of KAP3 and SOD1 in these specimens, affinity-purified rabbit anti-KAP3 antibody (0.05 μg/ml, diluted 1:200 in 1% bovine serum albumin-containing PBS, pH 7.4), mouse monoclonal antibody against human SOD1 (0.5 mg/ml, clone1$G_2$, MBL, Aichi, Japan) and sheep polyclonal antibody against human SOD1 (1:20,000, Calbiochem, Darmstadt, Germany) were used as primary antibodies. Immunohistochemical reaction was performed by a standard procedure. Antibody signal was visualized by the avidin–biotin–immunoperoxidase complex (ABC) method using the appropriate Vectastain ABC Kit (Vector Laboratories, Burlingame, CA, USA) and 3,3′-diaminobenzidine tetrahydrochloride (DAB; Dako, Glostrup, Denmark) as the chromogen.

## SUPPLEMENTARY MATERIAL

Supplementary Material is available at *HMG* online.

## ACKNOWLEDGEMENTS

We wish to thank the laboratory members for helpful suggestions and Tomoko Dai, Mariko Soda, Yumiko Shimazaki and Tadatoshi Makino for their technical support.

*Conflict of Interest statement*. None declared.

## FUNDING

This work was supported by research grants from RIKEN BSI, a Grant-in-Aid for Scientific Research on Priority Area (Advanced Brain Science Project) from the Ministry of Education, Culture, Sports, Science and Technology, NIBIO (Program for Promotion of Fundamental Studies in Health Sciences), a grant from Japan Foundation for Neuroscience and Mental Health and grants from the Ministry of Health, Labor and Welfare of Japan. Funding to pay the Open Access charge was provided by a grant from Ministry of Health, Labour and Welfare of Japan.

## REFERENCES

1. Boillee, S., Vande Velde, C. and Cleveland, D.W. (2006) ALS: a disease of motor neurons and their nonneuronal neighbors. *Neuron*, **52**, 39–59.
2. Pasinelli, P. and Brown, R.H. (2006) Molecular biology of amyotrophic lateral sclerosis: insights from genetics. *Nat. Rev. Neurosci.*, **7**, 710–723.
3. Shaw, B.F. and Valentine, J.S. (2007) How do ALS-associated mutations in superoxide dismutase 1 promote aggregation of the protein? *Trends Biochem. Sci.*, **32**, 78–85.
4. Barber, S.C., Mead, R.J. and Shaw, P.J. (2006) Oxidative stress in ALS: a mechanism of neurodegeneration and a therapeutic target. *Biochim. Biophys. Acta.*, **1762**, 1051–1067.
5. Wang, J., Xu, G. and Borchelt, D.R. (2002) High molecular weight complexes of mutant superoxide dismutase 1: age-dependent and tissue-specific accumulation. *Neurobiol. Dis.*, **9**, 139–148.
6. Shibata, N., Asayama, K., Hirano, A. and Kobayashi, M. (1996) Immunohistochemical study on superoxide dismutases in spinal cords from autopsied patients with amyotrophic lateral sclerosis. *Dev. Neurosci.*, **18**, 492–498.
7. Watanabe, M., Dykes-Hoberg, M., Culotta, V.C., Price, D.L., Wong, P.C. and Rothstein, J.D. (2001) Histological evidence of protein aggregation in mutant SOD1 transgenic mice and in amyotrophic lateral sclerosis neural tissues. *Neurobiol. Dis.*, **8**, 933–941.
8. Jonsson, P.A., Graffmo, K.S., Andersen, P.M., Brannstrom, T., Lindberg, M., Oliveberg, M. and Marklund, S.L. (2006) Disulphide-reduced superoxide dismutase-1 in CNS of transgenic amyotrophic lateral sclerosis models. *Brain*, **129**, 451–464.
9. Koyama, S., Arawaka, S., Chang-Hong, R., Wada, M., Kawanami, T., Kurita, K., Kato, M., Nagai, M., Aoki, M., Itoyama, Y. *et al.* (2006) Alteration of familial ALS-linked mutant SOD1 solubility with disease progression: its modulation by the proteasome and Hsp70. *Biochem. Biophys. Res. Commun.*, **343**, 719–730.
10. Goldstein, L.S. and Yang, Z. (2000) Microtubule-based transport systems in neurons: the roles of kinesins and dyneins. *Annu. Rev. Neurosci.*, **23**, 39–71.
11. Hirokawa, N. and Takemura, R. (2005) Molecular motors and mechanisms of directional transport in neurons. *Nat. Rev. Neurosci.*, **6**, 201–214.
12. De Vos, K.J., Grierson, A.J., Ackerley, S. and Miller, C.C. (2008) Role of axonal transport in neurodegenerative diseases. *Annu. Rev. Neurosci.*, **31**, 151–173.
13. Collard, J.F., Cote, F. and Julien, J.P. (1995) Defective axonal transport in a transgenic mouse model of amyotrophic lateral sclerosis. *Nature*, **375**, 61–64.
14. Williamson, T.L. and Cleveland, D.W. (1999) Slowing of axonal transport is a very early event in the toxicity of ALS-linked SOD1 mutants to motor neurons. *Nat. Neurosci.*, **2**, 50–56.
15. Hafezparast, M., Klocke, R., Ruhrberg, C., Marquardt, A., Ahmad-Annuar, A., Bowen, S., Lalli, G., Witherden, A.S., Hummerich, H., Nicholson, S. *et al.* (2003) Mutations in dynein link motor neuron degeneration to defects in retrograde transport. *Science*, **300**, 808–812.
16. Puls, I., Jonnakuty, C., LaMonte, B.H., Holzbaur, E.L., Tokito, M., Mann, E., Floeter, M.K., Bidus, K., Drayna, D., Oh, S.J. *et al.* (2003) Mutant dynactin in motor neuron disease. *Nat. Genet.*, **33**, 455–456.
17. Tateno, M., Sadakata, H., Tanaka, M., Itohara, S., Shin, R.M., Miura, M., Masuda, M., Aosaki, T., Urushitani, M., Misawa, H. *et al.* (2004) Calcium-permeable AMPA receptors promote misfolding of mutant SOD1 protein and development of amyotrophic lateral sclerosis in a transgenic mouse model. *Hum. Mol. Genet.*, **13**, 2183–2196.
18. Baqri, R., Charan, R., Schimmelpfeng, K., Chavan, S. and Ray, K. (2006) Kinesin-2 differentially regulates the anterograde axonal transports of acetylcholinesterase and choline acetyltransferase in *Drosophila*. *J. Neurobiol.*, **66**, 378–392.
19. Ray, K., Perez, S.E., Yang, Z., Xu, J., Ritchings, B.W., Steller, H. and Goldstein, L.S. (1999) Kinesin-II is required for axonal transport of choline acetyltransferase in *Drosophila*. *J. Cell Biol.*, **147**, 507–518.
20. Hirokawa, N. (2000) Stirring up development with the heterotrimeric kinesin KIF3. *Traffic*, **1**, 29–34.
21. Blusztajn, J.K. and Wurtman, R.J. (1983) Choline and cholinergic neurons. *Science*, **221**, 614–620.
22. McGee, R., Simpson, P., Christian, C., Mata, M., Nelson, P. and Nirenberg, M. (1978) Regulation of acetylcholine release from neuroblastoma × glioma hybrid cells. *Proc. Natl Acad. Sci. USA*, **75**, 1314–1318.
23. Tojima, T., Yamane, Y., Takahashi, M. and Ito, E. (2000) Acquisition of neuronal proteins during differentiation of NG108-15 cells. *Neurosci. Res.*, **37**, 153–161.
24. Johnston, J.A., Dalton, M.J., Gurney, M.E. and Kopito, R.R. (2000) Formation of high molecular weight complexes of mutant Cu, Zn-superoxide dismutase in a mouse model for familial amyotrophic lateral sclerosis. *Proc. Natl Acad. Sci. USA*, **97**, 12571–12576.
25. Puttaparthi, K., Wojcik, C., Rajendran, B., DeMartino, G.N. and Elliott, J.L. (2003) Aggregate formation in the spinal cord of mutant SOD1 transgenic mice is reversible and mediated by proteasomes. *J. Neurochem.*, **87**, 851–860.
26. Haraguchi, K., Hayashi, T., Jimbo, T., Yamamoto, T. and Akiyama, T. (2006) Role of the kinesin-2 family protein, KIF3, during mitosis. *J. Biol. Chem.*, **281**, 4094–4099.
27. Kato, S., Shimoda, M., Watanabe, Y., Nakashima, K., Takahashi, K. and Ohama, E. (1996) Familial amyotrophic lateral sclerosis with a two base pair deletion in superoxide dismutase 1: gene multisystem degeneration with intracytoplasmic hyaline inclusions in astrocytes. *J. Neuropathol. Exp. Neurol.*, **55**, 1089–1101.
28. Kato, S., Hayashi, H., Nakashima, K., Nanba, E., Kato, M., Hirano, A., Nakano, I., Asayama, K. and Ohama, E. (1997) Pathological

characterization of astrocytic hyaline inclusions in familial amyotrophic lateral sclerosis. *Am. J. Pathol.*, **151**, 611–620.
29. Kato, S. (2008) Amyotrophic lateral sclerosis models and human neuropathology: similarities and differences. *Acta Neuropathol.*, **115**, 97–114.
30. Rich, M.M., Wang, X., Cope, T.C. and Pinter, M.J. (2002) Reduced neuromuscular quantal content with normal synaptic release time course and depression in canine motor neuron disease. *J. Neurophysiol.*, **88**, 3305–3314.
31. Brandon, E.P., Lin, W., D'Amour, K.A., Pizzo, D.P., Dominguez, B., Sugiura, Y., Thode, S., Ko, C.P., Thal, L.J., Gage, F.H. *et al.* (2003) Aberrant patterning of neuromuscular synapses in choline acetyltransferase-deficient mice. *J. Neurosci.*, **23**, 539–549.
32. Wang, J., Xu, G., Li, H., Gonzales, V., Fromholt, D., Karch, C., Copeland, N.G., Jenkins, N.A. and Borchelt, D.R. (2005) Somatodendritic accumulation of misfolded SOD1-L126Z in motor neurons mediates degeneration: alphaB-crystallin modulates aggregation. *Hum. Mol. Genet.*, **14**, 2335–2347.
33. Dupuis, L., de Tapia, M., Rene, F., Lutz-Bucher, B., Gordon, J.W., Mercken, L., Pradier, L. and Loeffler, J.P. (2000) Differential screening of mutated SOD1 transgenic mice reveals early up-regulation of a fast axonal transport component in spinal cord motor neurons. *Neurobiol. Dis.*, **7**, 274–285.
34. Teuchert, M., Fischer, D., Schwalenstoecker, B., Habisch, H.J., Bockers, T.M. and Ludolph, A.C. (2006) A dynein mutation attenuates motor neuron degeneration in SOD1(G93A) mice. *Exp. Neurol.*, **198**, 271–274.
35. Kieran, D., Hafezparast, M., Bohnert, S., Dick, J.R., Martin, J., Schiavo, G., Fisher, E.M. and Greensmith, L. (2005) A mutation in dynein rescues axonal transport defects and extends the life span of ALS mice. *J. Cell Biol.*, **169**, 561–567.
36. Deacon, S.W., Serpinskaya, A.S., Vaughan, P.S., Lopez Fanarraga, M., Vernos, I., Vaughan, K.T. and Gelfand, V.I. (2003) Dynactin is required for bidirectional organelle transport. *J. Cell Biol.*, **160**, 297–301.
37. Pantelidou, M., Zographos, S.E., Lederer, C.W., Kyriakides, T., Pfaffl, M.W. and Santama, N. (2007) Differential expression of molecular motors in the motor cortex of sporadic ALS. *Neurobiol. Dis.*, **26**, 577–589.
38. Maselli, R.A., Wollman, R.L., Leung, C., Distad, B., Palombi, S., Richman, D.P., Salazar-Grueso, E.F. and Roos, R.P. (1993) Neuromuscular transmission in amyotrophic lateral sclerosis. *Muscle Nerve*, **16**, 1193–1203.
39. Balice-Gordon, R.J., Smith, D.B., Goldman, J., Cork, L.C., Shirley, A., Cope, T.C. and Pinter, M.J. (2000) Functional motor unit failure precedes neuromuscular degeneration in canine motor neuron disease. *Ann. Neurol.*, **47**, 596–605.
40. Shimizu, K., Kawabe, H., Minami, S., Honda, T., Takaishi, K., Shirataki, H. and Takai, Y. (1996) SMAP, an Smg GDS-associating protein having arm repeats and phosphorylated by Src tyrosine kinase. *J. Biol. Chem.*, **271**, 27013–27017.
41. Takeda, S., Yamazaki, H., Seog, D.H., Kanai, Y., Terada, S. and Hirokawa, N. (2000) Kinesin superfamily protein 3 (KIF3) motor transports fodrin-associating vesicles important for neurite building. *J. Cell Biol.*, **148**, 1255–1265.
42. Jimbo, T., Kawasaki, Y., Koyama, R., Sato, R., Takada, S., Haraguchi, K. and Akiyama, T. (2002) Identification of a link between the tumour suppressor APC and the kinesin superfamily. *Nat. Cell Biol.*, **4**, 323–327.
43. Teng, J., Rai, T., Tanaka, Y., Takei, Y., Nakata, T., Hirasawa, M., Kulkarni, A.B. and Hirokawa, N. (2005) The KIF3 motor transports N-cadherin and organizes the developing neuroepithelium. *Nat. Cell Biol.*, **7**, 474–482.
44. Urushitani, M., Kurisu, J., Tsukita, K. and Takahashi, R. (2002) Proteasomal inhibition by misfolded mutant superoxide dismutase 1 induces selective motor neuron death in familial amyotrophic lateral sclerosis. *J. Neurochem.*, **83**, 1030–1042.
45. Kumagai-Tohda, C., Tohda, M. and Nomura, Y. (1993) Increase in neurite formation and acetylcholine release by transfection of growth-associated protein-43 cDNA into NG108-15 cells. *J. Neurochem.*, **61**, 526–532.

Free Radical Biology & Medicine 47 (2009) 559–567

Contents lists available at ScienceDirect

Free Radical Biology & Medicine

journal homepage: www.elsevier.com/locate/freeradbiomed

Original Contribution

# Protective role of glutathione S-transferase A4 induced in copper/zinc-superoxide dismutase knockout mice

Daisaku Yoshihara [a], Noriko Fujiwara [a,*], Tomomi Ookawara [a], Shinsuke Kato [b], Haruhiko Sakiyama [a], Shunichi Yokoe [a], Hironobu Eguchi [a], Keiichiro Suzuki [a]

[a] Department of Biochemistry, Hyogo College of Medicine, 1-1 Mukogawa-cho, Nishinomiya, Hyogo 663-8501, Japan
[b] Department of Neuropathology, Institute of Neurological Sciences, Faculty of Medicine, Tottori University, Nishi-cho 36-1, Yonago 683-8504, Japan

ARTICLE INFO

*Article history:*
Received 30 January 2009
Revised 14 May 2009
Accepted 21 May 2009
Available online 28 May 2009

*Keywords:*
Superoxide dismutase
Oxidative stress
SOD1 knockout mice
Glutathione S-transferase
GSTA4
Iron
Free radicals

ABSTRACT

Copper/zinc-superoxide dismutase (SOD1) plays a protective role in cells by catalyzing the conversion of the superoxide anion into molecular oxygen and hydrogen peroxide. Although SOD1 knockout (KO) mice exhibit a reduced life span and an elevated incidence of dysfunctions in old age, young SOD1 KO mice grow normally and exhibit no abnormalities. This fact leads to the hypothesis that other antioxidative proteins prevent oxidative stress, compensating for SOD1. Differently expressed genes in 3-week-old SOD1 KO and littermate wild-type mice were explored. A gene remarkably elevated in SOD1 KO mouse kidneys was identified as the glutathione S-transferase Alpha 4 gene (*Gsta4*), which encodes the GSTA4 subunit. The GSTA4 protein level and activity were also significantly increased in SOD1 KO mouse kidneys. The administration of an iron complex, a free radical generator, induced GSTA4 expression in wild-type mouse kidneys. Iron deposition detected in SOD1 KO mouse kidney is thought to be an inducer of GSTA4. In addition, overexpression of mouse GSTA4 cDNA in human embryonic kidney cells decreased cell death caused by both 4-hydroxynonenal and hydrogen peroxide. These findings suggest that compensatory induced GSTA4 plays a protective role against oxidative stress in young SOD1 KO mouse kidneys.



Oxidative stress caused by accumulated reactive oxygen species (ROS)[1] is closely involved in a variety of pathological processes, including inflammation, cancer, neurodegenerative disorders, and aging. Most cells have a lot of defense systems for avoiding the toxic effects of ROS. A variety of antioxidative proteins and low-molecular-weight antioxidants are highly regulated to maintain cellular homeostasis. Among them, superoxide dismutase (SOD) is thought to play a central role because of its ability to scavenge superoxide anions, the primary ROS generated from molecular oxygen in cells. Mammals have three isozymes, Cu/Zn-SOD (SOD1), Mn-SOD (SOD2), and extracellular SOD (EC-SOD, SOD3). SOD1 is mainly localized in the cytosol and SOD2 is located exclusively in mitochondria. SOD3 protein is secreted into the extracellular space, where the majority of it becomes anchored to sulfated glycosaminoglycans in the tissue interstitium. Mutation of SOD1 causes familial amyotrophic lateral sclerosis (FALS), which is a neurological disease characterized by selective motor neurons in the brain and spinal cord. Several lines of transgenic mice that express the mutant human SOD1 linked with FALS develop progressive neurodegeneration and a phenotype that clearly resembles human FALS [1,2]. In contrast, young SOD1 knockout (KO) mice grow normally and exhibit no clear abnormalities except for a small body size and anemia [3]. However, adult or old SOD1 KO mice exhibit elevated incidences of alcohol-induced liver injury [4], hepatocarcinogenesis [5], ischemia/reperfusion-induced renal failure [6], hearing loss [7], lipid accumulation in the liver [8], and female infertility [9]. These phenotypes are probably caused by accumulated toxic organic peroxides such as lipid peroxides and unsaturated aldehydes resulting from the constitutive SOD1 deficiency.

The glutathione S-transferases (GSTs; EC 2.5.1.18) constitute a major group of phase II detoxification proteins that protect against a variety of reactive chemicals, such as chemotherapeutic agents and chemical carcinogens, and secondary metabolites during oxidative stress, such as α,β-unsaturated aldehydes, quinones, and hydroperoxides [10]. Mammalian cytosolic GSTs are all dimeric with subunits of 199–244 amino acids. Based on amino acid sequence similarities, at least seven classes of cytosolic GSTs are recognized in mammals, which are designated as Alpha, Mu, Pi, Sigma, Theta, Omega, and Zeta [10]. Among them, GSTA4-4, which is a homodimer of the GSTA4 subunit, belongs to the GST Alpha family and exhibits uniquely high glutathione conjugation activity toward 4-hydroxynonenal (4-HNE), an end-product of lipid peroxidation [11,12].

*Abbreviations:* ROS, reactive oxygen species; SOD, superoxide dismutase; FALS, familial amyotrophic lateral sclerosis; GST, glutathione S-transferase; 4-HNE, 4-hydroxynonenal; CDNB, 1-chloro-2,4-dinitrobenzene; MDA, malondialdehyde; Fe-NTA, ferric nitrilotriacetate; HEK293, human embryonic kidney 293; ARE, antioxidant-responsive element; Nrf2, nuclear factor E2-related factor 2.

* Corresponding author. Fax: +81 798 46 3164.
*E-mail address:* noriko-f@hyo-med.ac.jp (N. Fujiwara).

0891-5849/$ – see front matter © 2009 Elsevier Inc. All rights reserved.
doi:10.1016/j.freeradbiomed.2009.05.022

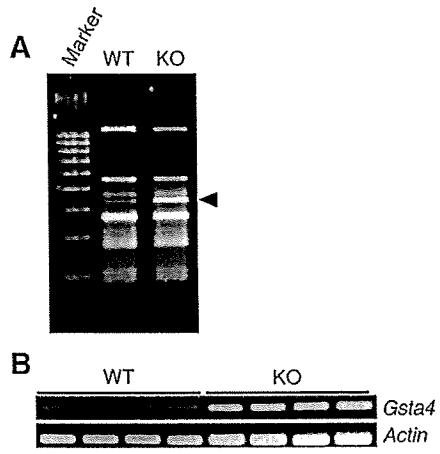


**Fig. 1.** Differential gene expression in SOD1 KO and WT mouse kidneys. (A) Differential banding patterns of genes isolated from SOD1 KO and WT mouse kidneys. The arrowhead indicates the more highly expressed gene in SOD1 KO mice. (B) RT-PCR analysis of *Gsta4* expression. Total RNAs were isolated from 3-week-old male SOD1 KO and WT mouse kidneys. PCR products were separated on a 2% agarose gel and stained with SYBR Green I.

The kidney plays an important role in the excretion of metabolic wastes and reabsorption of nutrients through blood filtration. The renal tubules tend to suffer oxidative stress from such metabolites including harmful agents through the active transport. Although SOD1 deficiency may further increase renal oxidative stress, clear abnormalities are not observed in young SOD1 KO mouse kidneys. Also, few differences in renal function between wild-type (WT) and SOD1 KO mice after ischemia/reperfusion at a young age were reported [6]. Accumulating studies have shown that SOD isoenzymes such as SOD2 and SOD3 probably do not cover a SOD1 deficiency [13] and that SOD1 and SOD3 have no overlapping roles, as seen with SOD1 and SOD3 double-KO mice [13]. These facts lead to the hypothesis that some unidentified antioxidative proteins protect against oxidative stress, compensating for SOD1.

In this study, we performed differential display analysis, using 3-week-old SOD1 KO and WT mouse kidneys, to search for compensatory working proteins. We found that the GSTA4 gene, *Gsta4*, which encodes the GSTA4 subunit, is remarkably induced in young SOD1 KO mouse kidneys. Thus, we focused on the investigation of the expression and roles of GSTA4 in SOD1 KO mouse kidneys by comparison with the expression of other antioxidative enzymes. In addition, we investigated whether ROS production mimicking SOD1 deficiency induces GSTA4 expression and whether GSTA4 overexpression has a protective effect against ROS-induced cell death. The results show that oxidative stress induces GSTA4 expression even in wild-type mouse kidneys and that the GSTA4-expressed cells have tolerance to 4-HNE- and hydrogen peroxide-induced cell death. Moreover, we found iron deposits in SOD1 KO mouse kidneys, which are probably related to the GSTA4 induction.

## Experimental procedures

### *Materials*

All chemicals used in this study were purchased from Wako Pure Chemical Industries Ltd., Nacalai Tesque, Inc., or Sigma–Aldrich, unless specified otherwise, and were of the highest grade available.

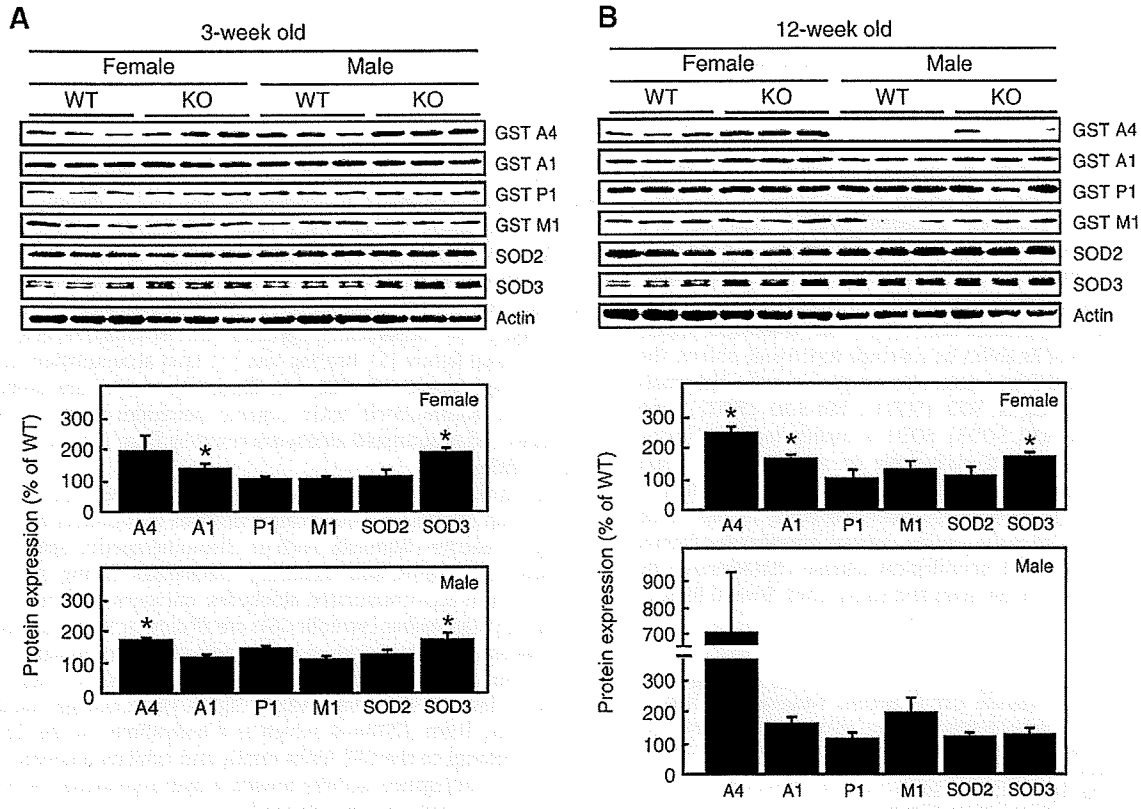


**Fig. 2.** GSTA4, GSTA1, GSTP1, GSTM1, SOD2, and SOD3 protein expression in SOD1 KO and WT mouse kidneys, at (A) 3 and (B) 12 weeks of age. The top shows the protein expression levels determined by Western blot analysis. The bottom (bar graphs) shows the fold (%) changes calculated against the protein levels in WT mice by densitometric scanning of the Western blots. The data are normalized to the expression levels of β-actin and expressed as means ± SEM (*$p<0.05$, compared with WT mice).

*Antibodies*

Polyclonal antibodies against human GSTA1, mouse GSTP1, mouse GSTM1, and β-actin were obtained from Oxford Biomedical Research, Stressgen, Upstream Biotechnology, Abcam, and Sigma–Aldrich, respectively. Antibodies against human SOD1 and rat SOD2 were kindly provided by Dr. Taniguchi (Osaka University, Osaka, Japan). Antibodies against mouse SOD3 were raised previously [14]. Horseradish peroxidase-conjugated goat anti-rabbit IgG and horseradish peroxidase-conjugated rabbit anti-goat IgG were purchased from Promega and DAKO, respectively.

*Experimental animals*

The mice used for this study were derived from breeding pairs of heterozygous SOD1-deficient (B6;129S-SOD1$^{tm1Leb}$) mice obtained from The Jackson Laboratory. The mice were backcrossed with C57BL/6J mice more than seven times before experiments. All breeding and genotyping were performed in a virus- and pathogen-free barrier facility at the Hyogo College of Medicine. The animals were maintained under an artificial 12/12-h light/dark cycle, as well as a constant temperature of 20–22°C, and had free access to food and distilled water. The genotype of each mouse was ascertained by polymerase chain reaction (PCR) of DNA isolated from a tail biopsy as described on The Jackson Laboratory Web site. All experiments were approved by the Hyogo College of Medicine Animal Care and Use Committee.

*Identification of differently expressed genes*

Screening of differently expressed genes in SOD1 KO and littermate WT mice was performed using a GeneFishing kit according to the manufacturer's instructions (Seegene). The PCR products were subjected to electrophoresis on a 2% agarose gel and then stained with SYBR Green I (Cambrex). The screened PCR products were cloned into the pT7Blue vector (Novagen) and subjected to cycle sequencing with a Model 3130XL automated sequencer (Applied Biosystems). The identity of each product was confirmed by sequence homology analysis using the Basic Alignment Search Tool.

*Production and purification of recombinant mouse GSTA4 protein*

Mouse GSTA4 (mGSTA4) cDNA was subcloned into the *Escherichia coli* expression vector pET-19b (Novagen) in frame with a six-histidine tag. After induction with 1 mM isopropyl-1-thio-*S*-d-galactopyranoside overnight at 27 °C in *E. coli* (BL21 strain), the cells were harvested. The cells were homogenized in a binding buffer (20 mM phosphate buffer, pH 7.4, containing 0.5 M NaCl and 20 mM imidazole) and then centrifuged at 10,000 g for 20 min at 4 °C. The recombinant mGSTA4 was purified by nickel-chelating chromatography on Ni–Sepharose 6 Fast Flow resin (GE Healthcare).

*Preparation of rabbit polyclonal antibodies to mouse GSTA4*

Keyhole limpet hemocyanin-coupled mGSTA4-specific peptide (residues 117–130) was obtained from Sigma–Aldrich. Immunization of rabbits and purification of IgG for mGSTA4 were carried out as described previously [15] with minor modifications. The anti-mGSTA4 antibody was purified on an affinity column coupled with the recombinant mGSTA4.

*RNA extraction and RT-PCR*

Total RNA was isolated from kidney samples using TRIzol reagent (Invitrogen). The expression of different mRNAs of interest was evaluated by reverse transcriptional polymerase chain reaction (RT-PCR) using a High Capacity RNA-to-cDNA kit (Applied Biosystems).

*Real-time PCR*

Relative quantitative analysis of mRNAs was performed using PCR with a SYBR Green Realtime PCR master mix (Toyobo) and an ABI Prism 7500HT Fast Real Time PCR system (Applied Biosystems) on MicroAmp optical 96-well reaction plates (Applied Biosystems). Amplification conditions were 1 min at 95°C, followed by 40 cycles of 15 s at 95°C and 1 min at 60°C.

*Protein extraction and Western blot analysis*

Tissues from mice or cells were homogenized in a cell lysis buffer (50 mM Tris–HCl buffer, pH 7.5, containing 0.25 M sucrose, 10 mM KCl, and 5 mM $MgCl_2$) containing a protease inhibitor cocktail (Nacalai Tesque). The homogenates were centrifuged at 15,000 g for 15 min at 4°C, and the supernatants were used for Western blot analysis and measurement of enzyme activities. Protein concentrations were determined using a BCA protein assay kit (Pierce) with bovine serum albumin as the standard. Aliquots of proteins (5–30 μg) were separated by SDS–polyacrylamide gel electrophoresis (SDS–PAGE) and then transferred onto a PVDF membrane under semidry conditions by means of a trans-blot (Bio-Rad). The membranes were blocked with 5% fat-free milk at room temperature for 1 h and then incubated overnight at 4°C with an appropriate primary antibody in 0.5% fat-free milk in Tris-buffered saline containing 0.05% Tween 20 (TBS-T). After being washed with TBS-T, each membrane was incubated with an appropriate secondary

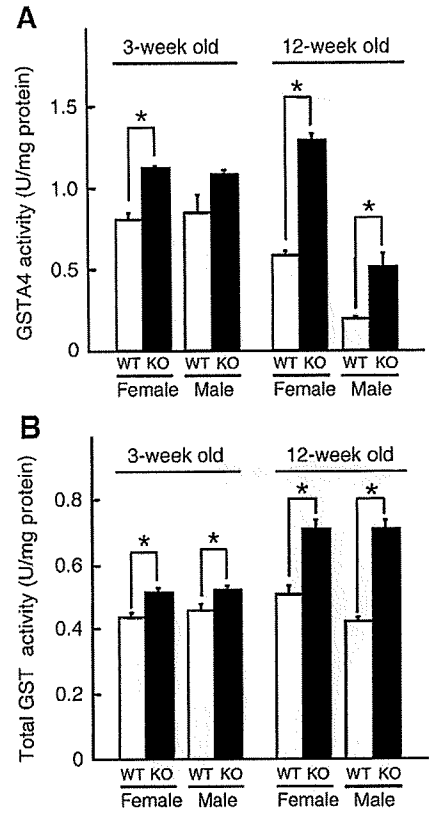


**Fig. 3.** Effects of the SOD1 deficiency on GSTA4 activity and total GST activity. (A) GSTA4 activity toward 4-HNE in 3- and 12-week-old mice. (B) Total GST activity toward CDNB in 3- and 12-week-old mice. The data are expressed as the means ± SEM for four or five animals (*$p < 0.05$, compared with WT mice of the same sex and age).

antibody at room temperature for 1 h. After another wash, a chemiluminescence method involving an ECL or an ECL Plus kit (GE Healthcare) was employed to detect peroxidase activity.

*Measurement of enzyme activities*

Total GST activity and GSTA4 activity against 1-chloro-2,4-dinitrobenzene (CDNB) and 4-HNE, respectively, were determined as described previously [16,17].

*Measurement of 4-HNE and malondialdehyde (MDA) levels*

The 4-HNE and MDA levels were determined using a Biotech LPO-586 kit (Oxis International) according to the manufacturer's protocol.

*Immunohistochemistry*

Mice were deeply anesthetized with sodium pentobarbital (0.1 ml/100 g of body wt) and then perfused with phosphate-buffered saline (PBS) via the aorta. After fixation with 4% paraformaldehyde in 0.1 M cacodylate buffer (pH 7.3), kidney specimens were embedded in paraffin, cut into 5-μm-thick sections, and then subjected to immunohistochemical analysis. Sections were deparaffinized and then washed in PBS. Normal serum homologous with a secondary antibody diluted in 1% BSA–PBS was used as the blocking reagent. Tissue sections were incubated with anti-GSTA4 for 18 h at 4°C. Bound antibody was visualized by the avidin–biotin–immunoperoxidase complex (ABC) method using an appropriate Vectastain Elite ABC rabbit IgG kit (Vector Laboratories) and 3,3′-diaminobenzidine tetrahydrochloride as the chromogen. The

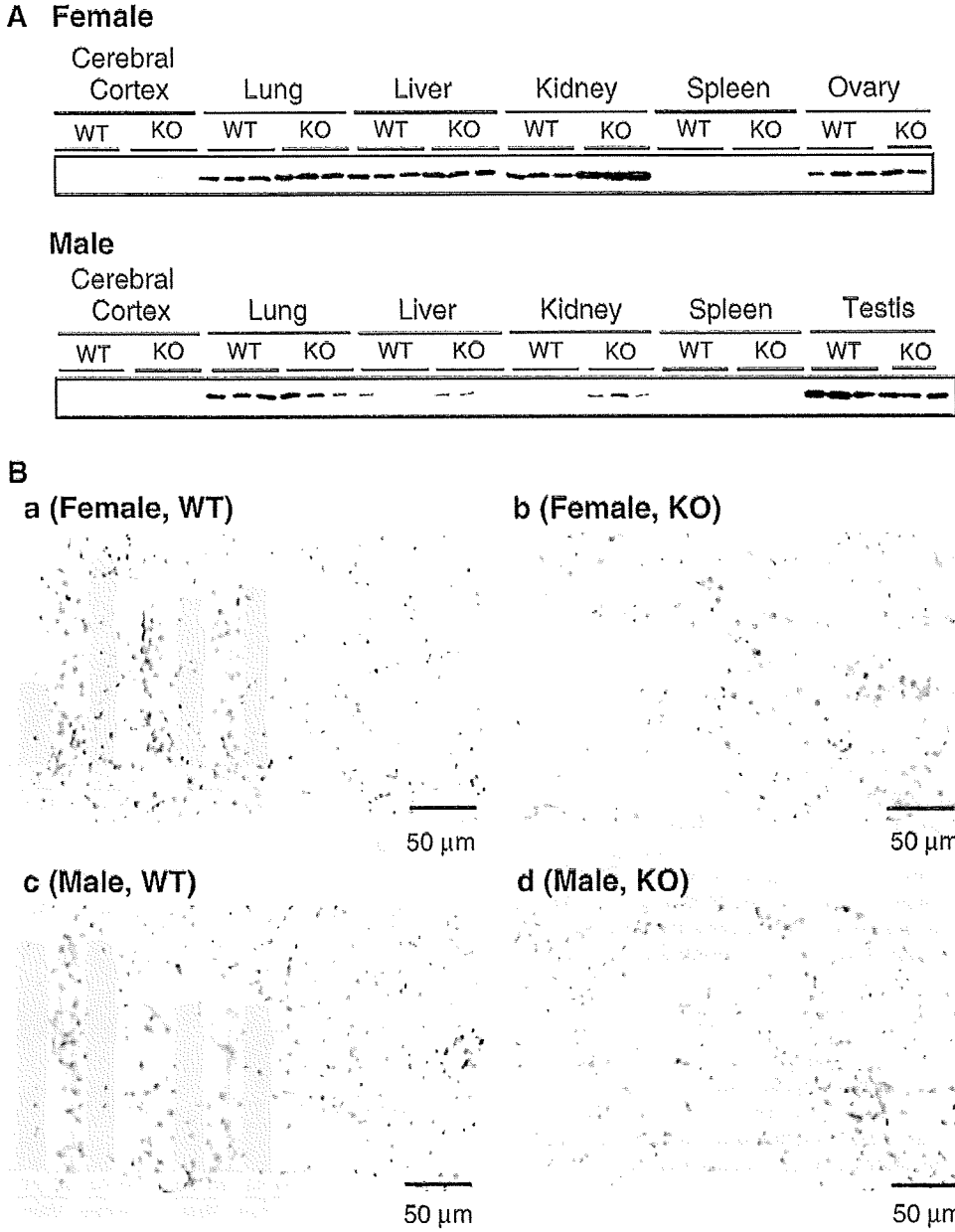


**Fig. 4.** (A) Expression of GSTA4 protein in various tissues in female (top) and male (bottom) 12-week-old SOD1 KO and WT mice. Fifteen micrograms of proteins from various tissues were subjected to Western blotting ($n=3$, except for ovary). (B) Immunohistochemical analysis of paraffin-embedded 12-week-old mouse kidney sections with detection by anti-mGATA4. (a) Female WT mouse, (b) female SOD1 KO mouse, (c) male WT mouse, (d) male SOD1 KO mouse. GSTA4 was preferentially expressed in the proximal tubules of female SOD1 KO mice.

endogenous peroxidase activity was quenched by incubation with 3% $H_2O_2$ for 30 min after the secondary antibody treatment.

*Prussian blue staining for tissue iron detection*

The paraffin sections were deparaffinized and then washed in Milli-Q (Millipore, Japan) water. The sections were incubated in 1% hydrochloric acid containing 1% potassium ferrocyanide for 20 min. After being washed with Milli-Q water, the sections were stained with nuclear fast red solution (Sigma) for 5 min.

*Preparation of a ferric nitrilotriacetate (Fe–NTA) solution and administration protocol*

The Fe–NTA solution was prepared immediately before use as previous described [18]. Female C57BL/6 J mice (7 weeks of age, 18–20 g) were purchased from Oriental Yeast Co. Ltd. Animals were given a single ip injection of Fe–NTA (7.5 mg iron/kg body wt), the same amount of NTA in the Fe–NTA solution or saline. The kidneys were extracted at 6 and 24 h after the injection.

*Cell culture*

The mouse proximal tubular epithelial cell line, mProx24, was kindly provided by Dr. Imai (Osaka University) [19]. The mProx24 cells and human embryonic kidney 293 (HEK293) cells were grown in K-1 medium (50/50 Ham's F-12/Dulbecco's modified Eagle's medium) and in Dulbecco's modified Eagle's medium, respectively, containing 100 units/ml penicillin and 100 μg/ml streptomycin supplemented with 10% heat-inactivated fetal bovine serum at 37°C under an atmosphere of 95% air and 5% $CO_2$.

*GSTA4 induction by hemin treatment*

The mProx24 cells were seeded into six-well plates ($5 \times 10^5$ cells/well) and incubated overnight in growth medium. After treatment with 10, 50, or 100 μM hemin for 6 or 24 h, the cells were liberated from the plates with ice-cold PBS. Total RNA was isolated from cell samples using TRIzol reagent and then subjected to semiquantitative RT-PCR.

*Detection of 4-HNE and MDA adducts in HEK293 cells*

HEK293 cells were transfected with either control pcDNA3.1 lacking an exogenous insert or pcDNA3.1 containing the mGSTA4 gene using Lipofectamine LTX reagent (Invitrogen) according to the manufacturer's instructions, and then hygromycin-resistant clones were selected. These stably transfected cells were seeded into 24-well flat-bottom plates ($2 \times 10^5$ cells/well) for cytotoxicity assay and into 6-well flat-bottom collagen-coated plates ($5 \times 10^5$ cells/well) for detection of 4-HNE and MDA adducts and grown for 24 to 36 h until confluent. The cells were treated with various concentrations of 4-HNE for 3 h or $H_2O_2$ for 24 h. Control cells were treated with the vehicle alone. For cytotoxicity assay, 100 μl of an MTT solution (0.5 mg/ml in PBS) was added to each well, followed by incubation for an additional 3 h. The blue MTT formazan precipitate was dissolved in acid–isopropanol and then measured with a microplate reader Model 550 (Bio-Rad) at the absorbance wavelength of 570 nm. For detection of 4-HNE and MDA adducts, cells were homogenized in a cell lysis buffer (50 mM Tris–HCl

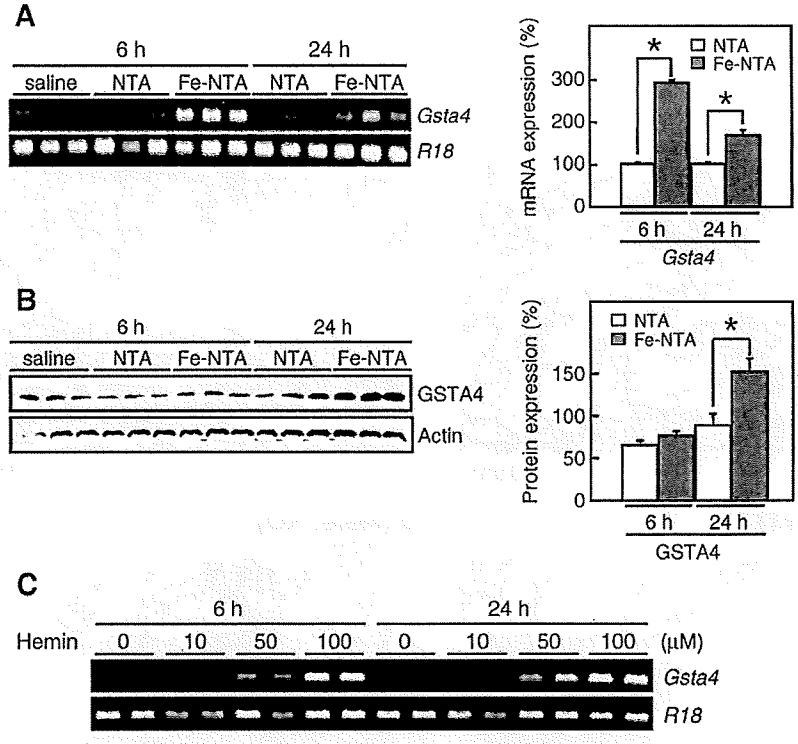


**Fig. 5.** (A) Effects of Fe–NTA treatment on *Gsta4* expression in 7-week-old female mouse kidneys. The left shows the expression of *Gsta4* by RT-PCR. PCR products were separated on a 2% agarose gel and stained with SYBR Green I. The right (bar graph) shows the fold (%) changes calculated against the mRNA level in the saline group by relative quantitative real-time PCR. The data are normalized to the expression levels of ribosomal protein S18 (R18) and expressed as means ± SEM (*$p<0.05$, compared with the NTA group with the same treatment time). (B) Effects of Fe–NTA treatment on the GSTA4 protein level in 7-week-old female mouse kidneys. Protein levels were normalized to those of β-actin. The left shows the GSTA4 protein levels determined by Western blot analysis. The right (bar graph) shows the fold (%) changes calculated against the protein levels in the saline group by densitometric scanning of the Western blots. The data are normalized to the expression level of β-actin and expressed as means ± SEM (*$p<0.05$, compared with the NTA group with the same treatment time). (C) Effects of hemin treatment on *Gsta4* expression in a mouse proximal tubular epithelial cell line (mProx24 cells).

buffer, pH 7.5, containing 0.25 M sucrose, 10 mM KCl, and 5 mM $MgCl_2$) with a protease inhibitor cocktail. The homogenates were centrifuged at 15,000 g for 15 min at 4 °C, and the supernatants were used for Western blot analysis. Forty micrograms of proteins was separated by SDS–PAGE and then subjected to Western blot analysis using anti-4-HNE (Nikken Seil), anti-MDA (Alpha Diagnostic), or anti-GSTA4.

*Statistical analysis*

Numerical values are expressed as means ± SEM. Student's *t* test was used for evaluation of statistical significance.

## Results

*GSTA4 is induced by the SOD1 deficiency*

We screened differently expressed genes in SOD1 KO and littermate WT mouse kidneys using a Gene-Fishing kit. As shown in Fig. 1A, we obtained one gene that was markedly up-regulated in 3-week-old male SOD1 KO mice compared with littermate male WT mice. This gene was cloned and identified as *Gsta4*, which encodes glutathione S-transferase Alpha 4. Moreover, RT-PCR using *Gsta4* gene primers proved that the GSTA4 mRNA level in SOD1 KO mouse kidneys was much higher than that in WT mouse kidneys (Fig. 1B). The real-time quantitative RT-PCR also showed threefold increases in GSTA4 mRNA levels in SOD1 KO mice compared with WT mice (data not shown). These results suggest that the *Gsta4* gene is induced in SOD1 KO mouse kidneys as one of the antioxidative proteins that compensate for SOD1.

We next examined the protein expression levels of GSTA4 and other antioxidative enzymes by Western blot analyses using total proteins isolated from kidneys derived from 3- and 12-week-old mice. Not only the GSTA4 protein but also the GSTA1 and SOD3 proteins were increased in SOD1 KO mice (Figs. 2A and B). In contrast, no differences in the protein levels of GSTP1, GSTM1, and SOD2 between SOD1 KO and WT mice of both genders and different ages were observed (Figs. 2A and B). We observed that the mRNA level of GSTA1, but not GSTP1 and GSTM1, is also increased in SOD1 KO mice as shown by real-time PCR (data not shown). In 12-week-old male mice, the GSTA4 expression in both SOD1 KO and WT was markedly decreased, although GSTA4 levels in SOD1 KO mice were still higher than in WT mice (Fig. 2B). These findings suggest that GSTA4 expression in male mice is limited to a young age.

The alteration in the amount of the GSTA4 protein could affect the enzyme activity, and hence GSTA4 activity and total GST activity, using 4-HNE and CDNB, respectively, as the substrates, were measured, because CDNB is a common substrate for most forms of GST and 4-HNE is more specific to GSTA4 [20]. As shown in Fig. 3A, the GSTA4 activity in SOD1 KO mice was higher than that in WT mice, the levels being similar in both female and male mice at 3 weeks of age. In contrast, the activity in male mice was significantly lower than that in female mice at 12 weeks of age although the GSTA4 activity in SOD1 KO mice was higher than that in WT mice. The GSTA4 activity in male SOD1 KO mice was identical to that in female WT mice at 12 weeks. This GSTA4 activity in 12-week-old mice might be reflected by the GSTA4 expression pattern (Fig. 2B). As for total GST activity, higher and similar levels were observed in both female and male SOD1 KO mice (Fig. 3B).

It has been reported that GSTA4 is induced by lipid peroxide accumulation, especially by 4-HNE [21]. Thus, we supposed that lipid peroxidation increases in SOD1 KO mouse kidneys with SOD1 deficiency. However, the levels of lipid peroxides, i.e., MDA and 4-HNE, were not increased in either 3- or 12-week-old SOD1 KO mouse kidneys (data not shown).

*GSTA4 is induced in proximal tubules in SOD1 KO mice*

The effects of SOD1 deficiency on the tissue distribution of GSTA4 expression were examined by Western blot analysis. As shown in

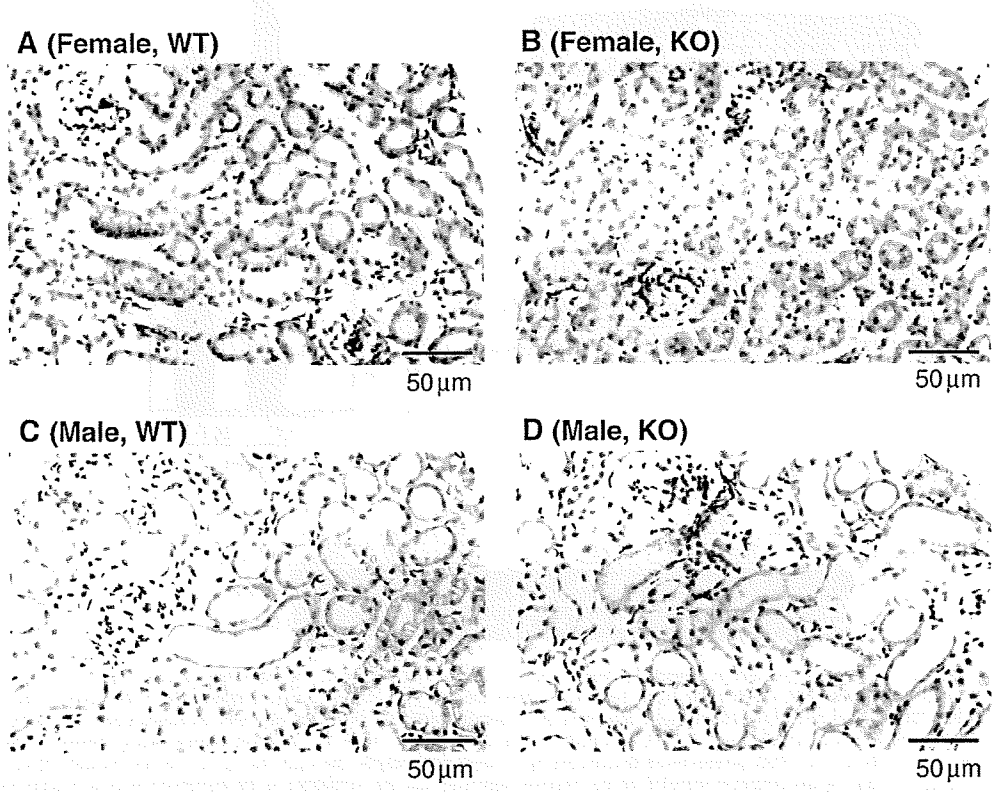


**Fig. 6.** Detection of iron deposits of paraffin-embedded 12-week-old mouse kidney sections. (a) Female WT mouse, (b) female SOD1 KO mouse, (c) male WT mouse, (d) male SOD1 KO mouse.

Fig. 4A, remarkable increases in GSTA4 expression were observed in kidney, whereas slight increases were observed in cerebral cortex, lung, and liver. We further examined the cell population exhibiting GSTA4 induction in SOD1 KO mouse kidneys by immunohistochemistry. In the 12-week-old SOD1 KO female mouse kidneys, GSTA4 was preferentially detected in the cortex area (data not shown), and the proximal tubules were more intensively labeled compared with WT mice and SOD1 KO male mice (Fig. 4B). In contrast, the glomeruli were not immunostained.

*GSTA4 is induced by iron load*

The iron complex Fe–NTA is a good ROS inducer and its administration causes acute renal tubular injury [18,22]. The effect of Fe–NTA injection on *Gsta4* gene expression was examined by using normal C57BL/6J mice. As a result, it was found that the GSTA4 mRNA level was drastically increased after 6 h (Fig. 5A), and the GSTA4 protein was increased at 24 h after Fe–NTA injection (Fig. 5B). Administration of cisplatin, which is another ROS generator [23], also induced the *Gsta4* gene (data not shown). Because the Fe–NTA injection could also load iron into the kidney, we examined whether iron loading induces GSTA4 in a mouse proximal tubular epithelial cell line (mProx24 cells). As shown in Fig. 5C, hemin treatment induced GSTA4 mRNA in a dose-dependent manner.

*Iron deposition is observed in SOD1 KO mouse kidneys*

The results shown in Fig. 5 suggested that GSTA4 induction is associated with iron overload. Thus, the kidney tissue iron level was compared between SOD1 KO and WT mice. As shown in Fig. 6, iron deposits, giving a positive reaction with Prussian blue staining, were detected in the renal proximal tubules, especially in female SOD1 KO mice.

*GSTA4 has a protective role against cytotoxicity caused by 4-HNE and $H_2O_2$*

We finally examined whether GSTA4 induction plays a protective role in 4-HNE- or hydrogen peroxide-induced cell death using HEK293 cells transfected with mGSTA4. The overexpression of mGSTA4 reduced the cell death caused by both 4-HNE (Fig. 7A) and $H_2O_2$ (Fig. 7B) and inhibited the formation of 4-HNE protein adducts (Fig. 7C) and MDA protein adducts (Fig. 7D) in 4-HNE- and $H_2O_2$-treated cells, respectively. These results clearly demonstrate that GSTA4 conjugates with and eliminates the 4-HNE and MDA in cells, and therefore contributes to a protection from ROS-induced cytotoxic effects.

## Discussion

In this study we demonstrated that the GSTA4 gene, protein level, and activity are remarkably increased in young SOD1 KO mouse kidneys (Figs. 1–3). The clear induction of GSTA4 was limited to kidney among various organs (Fig. 4A) and was particularly observed in proximal tubular cells of female mice (Fig. 4B). Administration of the iron complex Fe–NTA induced GSTA4 mRNA and protein expression in wild-type mice (Fig. 5). Desmots et al. also showed that iron overload caused by feeding an Fe-containing diet for 8 months induced the GSTA4 protein but strongly decreased GSTA1 and GSTM1 expression in mouse kidneys [24]. These findings suggest that GSTA4 induction is one of the compensatory regulation systems protecting cells from ROS produced on iron exposure. The reports showing increases in the iron contents of liver and serum [13] and enhanced hemolysis caused by the much shorter erythrocyte turnover [3] observed in SOD1 KO mice led to our speculation illustrated in Fig. 8. The higher iron deposits in SOD1 KO mouse kidney (Fig. 6) probably caused by the enhanced hemolysis would lead to ROS production and GSTA4 induction. A detailed investigation of iron metabolism in SOD1 KO mouse kidney is under way in our laboratory.

The substrate of GSTA4, 4-HNE, is a strong toxic lipid-derived aldehyde formed through oxidative cleavage of linoleic and arachidonic acids in cells [25] and is associated with the etiology of a variety of degenerative disorders such as atherosclerosis [26], Parkinson disease [27], and Alzheimer disease [28]. GSTA4 KO mice are reported to exhibit lower litter size, higher fat content in bones, and greater susceptibility to bacterial infection [29]. In addition, the GSTA4 KO mice had a significantly shorter survival time when chronically treated with low doses of paraquat [29], which indicates that GSTA4 has a defensive role against oxidative stress. It is noteworthy that a remarkable induction of several antioxidative enzymes, including SOD1, SOD2, and catalase, was observed in the GSTA4 KO mouse liver

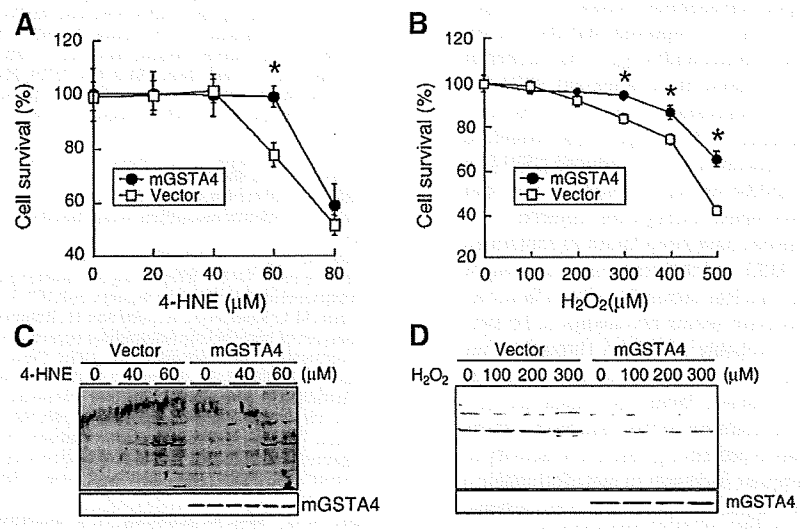


**Fig. 7.** Effects of overexpression of mGSTA4 on (A) 4-HNE- and (B) $H_2O_2$-induced cell death. Closed circles, HEK293 cells stably transfected with mGSTA4 cDNA. Open squares, HEK293 cells stably transfected with the empty vector (*$p<0.05$, compared with viability of the HEK293 clone transfected with the empty vector treated with the same concentrations of 4-HNE or $H_2O_2$). (C) Top: 4-HNE protein adducts in HEK293 cells transfected with mGSTA4 cDNA or the vector detected by Western blot analysis with anti-4-HNE. Bottom: Mouse GSTA4 proteins were detected only in HEK293 cells transfected with mGSTA4 cDNA. (D) Top: MDA protein adducts in HEK293 cells transfected with mGSTA4 cDNA or the vector detected by Western blot analysis with anti-MDA. Bottom: Mouse GSTA4 proteins were detected only in HEK293 cells transfected with mGSTA4 cDNA.

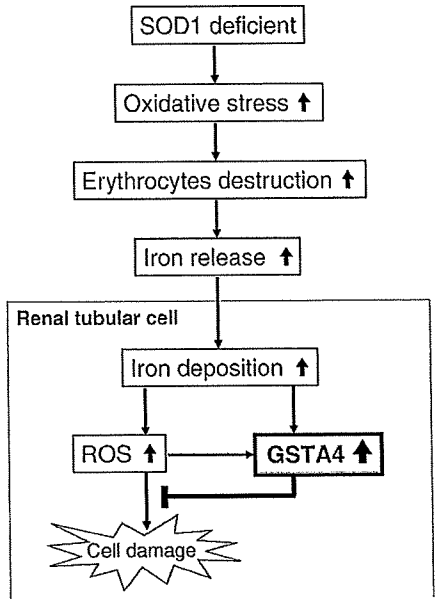


**Fig. 8.** Proposed mechanism of GSTA4 induction in SOD1 KO mouse kidney. SOD1 deficiency could accelerate the destruction of erythrocytes and the resultant iron release. The increased serum iron would be absorbed into kidney cells and the resultant accumulated iron would induce GSTA4 expression to protect the cells against oxidative stress.

[29]. SOD1 and GSTA4 probably compensate for the mutual deficiency. Cheng et al. [30] reported that human myeloid HL-60 cells transfected with mGSTA4 were protected from 4-HNE-induced apoptosis through a block in JNK-mediated signaling. We also found that human kidney cells transfected with mGSTA4 were protected from not only 4-HNE- but also hydrogen peroxide-induced cell death (Fig. 7). The lower levels of 4-HNE and MDA protein adducts in the mGSTA4-transfected cells (Figs. 7C and D) indicate that GSTA4 detoxified these lipid peroxides in the cells. Although an increase in the contents of GSTA4 inducers, i.e., MDA and 4-HNE, was not observed, the induced GSTA4 in cooperation with other antioxidative enzymes such as SOD3 and GSTA1 probably maintains the normal concentrations of these toxic oxidant metabolites in young SOD1 KO mouse kidneys. GSTA4 would increase the excretion rate of lipid peroxidation products as conjugates into urine. In fact, Sentman et al. [13] reported that the urinary excretion of the isoprostane 8-iso-prostaglandin $F_{2\alpha}$, a biomarker of lipid peroxidation, significantly increased in 12-week-old SOD1 KO mice. Because prostaglandins and isoprostanes are GST substrates [10], the increase in urinary excretion of the isoprostane would be through glutathione conjugation reactions by the induced GSTA4 in kidney. Precise studies on how GSTA4 works to eliminate the lipid peroxidation products in SOD1 KO mouse kidneys are required.

A substantial number of GST genes have been found to contain an antioxidant-responsive element (ARE), and their expression is thought to be regulated by the ARE/Nrf2 (nuclear factor E2-related factor 2) system [31]. However, their expression seems not always to be synchronized. Each GST isozyme is probably regulated through other transcriptional factors, such as activator protein 1, signal transducer and activator of transcription, or nuclear factor-κB, which are also involved in oxidative stress [31], in addition to the ARE/Nrf2 system. Remarkable changes in antioxidative protein expression or activity in SOD1 KO mice reported so far comprise increases in metallothionein-I and -II [32] and decreases in iron regulatory protein 1 [33], carbonic anhydrase III [5,34] proteins, and GPx activity [5,13,35]. However, Yamanobe et al. reported that the protein levels of antioxidative enzymes, i.e., glutathione reductase, peroxiredoxin 1 (Prx1), Prx4, glutathione peroxidase 1, aldose reductase, and aldehyde reductase, were not increased in SOD1 KO mouse kidneys [6]. Further studies are needed to clarify the regulation mechanism causing the alteration in expression of various antioxidative proteins, including GST isozymes under oxidative stress, and the differences in GSTA4 expression between genders and ages in SOD1 KO and even WT mice.

In conclusion, the findings herein show that the *Gsta4* gene is induced by ROS production, such as under the condition of a SOD1 deficiency, and that the overexpression of GSTA4 protects cells from 4-HNE- or hydrogen peroxide-induced cell death. These findings suggest that GSTA4 plays an important role by protecting against oxidative stress in young SOD1 KO mouse kidneys.

## Acknowledgments

We are grateful to Dr. Enyu Imai for kindly providing the mProx24 cells. This work was supported by a Grant-in-Aid for Scientific Research (20590320, K.S.); a Hitech Research Center grant from the Ministry of Education, Culture, Sports, Science and Technology of Japan; a Grant-in-Aid for Graduate Students, Hyogo College of Medicine (D.Y.); the Japan Foundation for Applied Enzymology (N.F.); and a Grant from The Research Group on Development of Novel Therapeutics for ALS of the Ministry of Health, Labour and Welfare of Japan (S.K.).

## References

[1] Gurney, M. E.; Pu, H.; Chiu, A. Y.; Dal Canto, M. C.; Polchow, C. Y.; Alexander, D. D.; Caliendo, J.; Hentati, A.; Kwon, Y. W.; Deng, H. X.; Chen, W.; Zhai, P.; Sufit, R. L.; Siddique, T. Motor neuron degeneration in mice that express a human Cu,Zn superoxide dismutase mutation. *Science* **264:**1772–1775; 1994.

[2] Ripps, M. E.; Huntley, G. W.; Hof, P. R.; Morrison, J. H.; Gordon, J. W. Transgenic mice expressing an altered murine superoxide dismutase gene provide an animal model of amyotrophic lateral sclerosis. *Proc. Natl. Acad. Sci. USA* **92:** 689–693; 1995.

[3] Iuchi, Y.; Okada, F.; Onuma, K.; Onoda, T.; Asao, H.; Kobayashi, M.; Fujii, J. Elevated oxidative stress in erythrocytes due to a SOD1 deficiency causes anaemia and triggers autoantibody production. *Biochem. J.* **402:**219–227; 2007.

[4] Kessova, I. G.; Ho, Y. S.; Thung, S.; Cederbaum, A. I. Alcohol-induced liver injury in mice lacking Cu, Zn-superoxide dismutase. *Hepatology* **38:**1136–1145; 2003.

[5] Elchuri, S.; Oberley, T. D.; Qi, W.; Eisenstein, R. S.; Jackson, R. L.; Van, R. H.; Epstein, C. J.; Huang, T. T. CuZnSOD deficiency leads to persistent and widespread oxidative damage and hepatocarcinogenesis later in life. *Oncogene* **24:** 367–380; 2005.

[6] Yamanobe, T.; Okada, F.; Iuchi, Y.; Onuma, K.; Tomita, Y.; Fujii, J. Deterioration of ischemia/reperfusion-induced acute renal failure in SOD1-deficient mice. Free Radic. *Res.* **41:**200–207; 2007.

[7] Ohlemiller, K. K.; McFadden, S. L.; Ding, D. L.; Flood, D. G.; Reaume, A. G.; Hoffman, E. K.; Scott, R. W.; Wright, J. S.; Putcha, G. V.; Salvi, R. J. Targeted deletion of the cytosolic Cu/Zn-superoxide dismutase gene (Sod1) increases susceptibility to noise-induced hearing loss. *Audiol. Neurootol.* **4:**237–246; 1999.

[8] Uchiyama, S.; Shimizu, T.; Shirasawa, T. CuZn-SOD deficiency causes ApoB degradation and induces hepatic lipid accumulation by impaired lipoprotein secretion in mice. *J. Biol. Chem.* **281:**31713–31719; 2006.

[9] Matzuk, M. M.; Dionne, L.; Guo, Q.; Kumar, T. R.; Lebovitz, R. M. Ovarian function in superoxide dismutase 1 and 2 knockout mice. *Endocrinology* **139:**4008–4011; 1998.

[10] Hayes, J. D.; Flanagan, J. U.; Jowsey, I. R. Glutathione transferases. *Annu. Rev. Pharmacol. Toxicol.* **45:**51–88; 2005.

[11] Jensson, H.; Guthenberg, C.; Alin, P.; Mannervik, B. Rat glutathione transferase 8-8, an enzyme efficiently detoxifying 4-hydroxyalk-2-enals. *FEBS Lett.* **203:**207–209; 1986.

[12] Nanduri, B.; Zimniak, P. Role of active-site residues 107 and 108 of glutathione S-transferase mGSTA4-4 in determining the catalytic properties of the enzyme for 4-hydroxynonenal. *Arch. Biochem. Biophys.* **362:**167–174; 1999.

[13] Sentman, M. L.; Granstrom, M.; Jakobson, H.; Reaume, A.; Basu, S.; Marklund, S. L. Phenotypes of mice lacking extracellular superoxide dismutase and copper- and zinc-containing superoxide dismutase. *J. Biol. Chem.* **281:**6904–6909; 2006.

[14] Ookawara, T.; Kizaki, T.; Ohishi, S.; Yamamoto, M.; Matsubara, O.; Ohno, H. Purification and subunit structure of extracellular superoxide dismutase from mouse lung tissue. *Arch. Biochem. Biophys.* **340:**299–304; 1997.

[15] Fujiwara, N.; Nakano, M.; Kato, S.; Yoshihara, D.; Ookawara, T.; Eguchi, H.; Taniguchi, N.; Suzuki, K. Oxidative modification to cysteine sulfonic acid of Cys111 in human copper–zinc superoxide dismutase. *J. Biol. Chem.* **282:**35933–35944; 2007.

[16] Habig, W. H.; Pabst, M. J.; Jakoby, W. B. Glutathione S-transferases: the first enzymatic step in mercapturic acid formation. *J. Biol. Chem.* **25:**7130–7139; 1974.

[17] Alin, P.; Danielson, U. H.; Mannervik, B. 4-Hydroxyalk-2-enals are substrates for glutathione transferase. *FEBS Lett.* **179:**267–270; 1985.

[18] Kawabata, T.; Ma, Y.; Yamador, I.; Okada, S. Iron-induced apoptosis in mouse renal proximal tubules after an injection of a renal carcinogen, iron-nitrilotriacetate. *Carcinogenesis* **18:**1389–1394; 1997.

[19] Takaya, K.; Koya, D.; Isono, M.; Sugimoto, T.; Sugaya, T.; Kashiwagi, A.; Haneda, M. Involvement of ERK pathway in albumin-induced MCP-1 expression in mouse proximal tubular cells. *Am. J. Physiol. Renal Physiol.* **284**:F1037–F1045; 2003.

[20] Hayes, J. D.; Pulford, D. J. The glutathione S-transferase supergene family: regulation of GST and the contribution of the isoenzymes to cancer chemoprotection and drug resistance. *Crit. Rev. Biochem. Mol. Biol.* **30**:445–600; 1995.

[21] Raza, H.; Robin, M. A.; Fang, J. K.; Avadhani, N. G. Multiple isoforms of mitochondrial glutathione S-transferases and their differential induction under oxidative stress. *Biochem. J.* **366**:45–55; 2002.

[22] Tanaka, T.; Nishiyama, Y.; Okada, K.; Satoh, K.; Fukuda, A.; Uchida, K.; Osawa, T.; Hiai, H.; Toyokuni, S. Over-expression of glutathione S-transferase Yp isozyme and concomitant down-regulation of Ya isozyme in renal cell carcinoma of rats induced by ferric nitrilotriacetate. *Carcinogenesis* **19**:897–903; 1998.

[23] Zhou, H.; Kato, A.; Miyaji, T.; Yasuda, H.; Fujigaki, Y.; Yamamoto, T.; Yonemura, K.; Takebayashi, S.; Mineta, H.; Hishida, A. Urinary marker for oxidative stress in kidneys in cisplatin-induced acute renal failure in rats. *Nephrol. Dial. Transplant.* **21**:616–623; 2006.

[24] Desmots, F.; Rissel, M.; Pigeon, C.; Loyer, P.; Loreal, O.; Guillouzo, A. Differential effects of iron overload on GST isoform expression in mouse liver and kidney and correlation between GSTA4 induction and overproduction of free radicals. *Free Radic. Biol. Med.* **32**:93–101; 2002.

[25] Esterbauer, H.; Schaur, R. J.; Zollner, H. Chemistry and biochemistry of 4-hydroxynonenal, malonaldehyde and related aldehydes. *Free Radic. Biol. Med.* **11**:81–128; 1991.

[26] Uchida, K.; Toyokuni, S.; Nishikawa, K.; Kawakishi, S.; Oda, H.; Hiai, H.; Stadtman, E. R. Michael addition-type 4-hydroxy-2-nonenal adducts in modified low-density lipoproteins: markers for atherosclerosis. *Biochemistry* **33**:12487–12494; 1994.

[27] Yoritaka, A.; Hattori, N.; Uchida, K.; Tanaka, M.; Stadtman, E. R.; Mizuno, Y. Immunohistochemical detection of 4-hydroxynonenal protein adducts in Parkinson disease. *Proc. Natl. Acad. Sci. USA* **93**:2696–2701; 1996.

[28] Lovell, M. A.; Ehmann, W. D.; Mattson, M. P.; Markesbery, W. R. Elevated 4-hydroxynonenal in ventricular fluid in Alzheimèr's disease. *Neurobiol. Aging* **18**: 457–461; 1997.

[29] Engle, M. R.; Singh, S. P.; Czernik, P. J.; Gaddy, D.; Montague, D. C.; Ceci, J. D.; Yang, Y.; Awasthi, S.; Awasthi, Y. C.; Zimniak, P. Physiological role of mGSTA4–4, a glutathione S-transferase metabolizing 4-hydroxynonenal: generation and analysis of mGsta4 null mouse. *Toxicol. Appl. Pharmacol.* **194**:296–308; 2004.

[30] Cheng, J. Z.; Singhal, S. S.; Sharma, A.; Saini, M.; Yang, Y.; Awasthi, S.; Zimniak, P.; Awasthi, Y. C. Transfection of mGSTA4 in HL-60 cells protects against 4-hydroxynonenal-induced apoptosis by inhibiting JNK-mediated signaling. *Arch. Biochem. Biophys.* **392**:197–207; 2001.

[31] Desmots, F.; Rauch, C.; Henry, C.; Guillouzo, A.; Morel, F. Genomic organization, 5′-flanking region and chromosomal localization of the human glutathione transferase A4 gene. *Biochem. J.* **336**:437–442; 1988.

[32] Ghoshal, K.; Majumder, S.; Li, Z.; Bray, T. M.; Jacob, S. T. Transcriptional induction of metallothionein-I and -II genes in the livers of Cu,Zn-superoxide dismutase knockout mice. *Biochem. Biophys. Res. Commun.* **264**:735–742; 1999.

[33] Starzynski, R. R.; Lipinski, P.; Drapier, J. C.; Diet, A.; Smuda, E.; Bartlomiejczyk, T.; Gralak, M. A.; Kruszewski, M. Down-regulation of iron regulatory protein 1 activities and expression in superoxide dismutase 1 knock-out mice is not associated with alterations in iron metabolism. *J. Biol. Chem.* **280**:4207–4212; 2005.

[34] Elchuri, S.; Naeemuddin, M.; Sharpe, O.; Robinson, W. H.; Huang, T. T. Identification of biomarkers associated with the development of hepatocellular carcinoma in CuZn superoxide dismutase deficient mice. *Proteomics* **7**:2121–2129; 2007.

[35] Lei, X. G.; Zhu, J. H.; McClung, J. P.; Aregullin, M.; Roneker, C. A. Mice deficient in Cu, Zn-superoxide dismutase are resistant to acetaminophen toxicity. *Biochem. J.* **399**: 455–461; 2006.

J Neuropathol Exp Neurol


Vol. 68, No. 1
January 2009
pp. 37–47

ORIGINAL ARTICLE

# Nuclear TAR DNA Binding Protein 43 Expression in Spinal Cord Neurons Correlates With the Clinical Course in Amyotrophic Lateral Sclerosis

Hisae Sumi, MD, PhD, Shinsuke Kato, MD, PhD, Yuko Mochimaru, Harutoshi Fujimura, MD, PhD, Masaki Etoh, MD, PhD, and Saburo Sakoda, MD, PhD

**Abstract**

TAR DNA binding protein 43 (TDP-43) has been considered a signature protein in frontotemporal dementia and amyotrophic lateral sclerosis (ALS), but not in ALS associated with the superoxide dismutase 1 (*SOD1*) gene mutations (ALS1). To clarify how TDP may be involved in ALS pathogenesis, clinical and pathological features in cases of sporadic ALS ([SALS] n = 18) and ALS1 (n = 6) were analyzed. In SALS patients with rapid clinical courses, TDP mislocalization (i.e. cytoplasmic staining and TDP-positive cytoplasmic inclusions) in anterior horn cells was frequent. In SALS patients with slow clinical courses, TDP-43 mislocalization was rare. In an ALS1 patient with the *SOD1* gene mutation C111Y, there were numerous TDP-positive inclusions and colocalization of SOD1 and TDP. In mutant SOD1 transgenic (G93A) mice at the end stage (median, 256 days), TDP-positive inclusions and TDP colocalization with SOD1 were also observed; nuclear TDP-43 immunoreactivity was highly correlated with life span in these mice. In both humans and mice, nuclei that stained strongly for TDP were large and circular; weakly stained nuclei were atrophic or deformed. In conclusion, low levels of TDP expression in the nucleus cor relate with a rapid clinical course in SALS and in ALS1 model mice, suggesting that nuclear TDP may play a protective role against motor neuron death resulting from different underlying etiologies.

**Key Words**: Amyotrophic lateral sclerosis, ALS, Anterior horn cell, ALS1, G93A transgenic mice, Lewy body–like hyaline inclusion, SOD1, TDP-43.

## INTRODUCTION

Amyotrophic lateral sclerosis (ALS) is a fatal motor neuron disease that causes progressive motor paralysis. The underlying pathogenetic mechanisms are largely unknown in 90% of ALS patients, that is, those with sporadic ALS (SALS). Of the 10% of ALS cases with familial ALS (FALS), approximately one fifth are associated with a mutation in the superoxide dismutase 1 (*SOD1*) gene; these patients are classified as ALS1 (1, 2). The pathogenesis of ALS1 is thought to involve aggregation of mutant SOD1 and subsequent oxidative stress (3). Another rare cause of juvenile autosomal recessive FALS is the gene that encodes ALS2, also known as alsin (4, 5). In most cases of FALS, however, the causative gene has not been identified because of low penetrance.

TAR DNA binding protein 43 (TDP-43), a nuclear protein, contains 2 fully functional RNA recognition motif domains and a C-terminal region that is capable of binding directly to several proteins of the heterogeneous nuclear ribonucleoprotein family (6–8); these ribonucleoproteins have a variety of functions including the modification, stabilization, and transport of RNA. The TDP modifies the splicing of exon 9 of the cystic fibrosis transmembrane conductance regulator gene (9) and of exon 3 of the apolipoprotein A-II gene (10). Recently, it also has been reported that loss of TDP in vitro results in nuclear dysmorphism, misregulation of the cell cycle, and apoptosis (11).

Neuronal inclusions, such as Lewy body–like hyaline inclusions (LBHIs), or the aggregation of mutant SOD1 in ALS1 (3, 12) are known to be important pathological features in the pathogenesis of neurodegenerative diseases. The TDP is a component of the ubiquitin-positive inclusions and neurites observed in frontotemporal dementia and ALS (13, 14). The TDP-positive round or filamentous inclusions in the cytoplasm and mislocalization of TDP from the nucleus to the cytoplasm have been observed in all cases of SALS (15) and FALS, but not in ALS1 (16, 17). A novel missense mutation in TDP was recently identified as causative in familial motor neuron disease and SALS (18, 19). Although the concept of TDP proteinopathy has been suggested (14, 20), the presence of TDP-positive inclusions in other diseases, including hippocampal sclerosis, Alzheimer disease (21), Parkinson disease (22), Pick disease (23), and neoplastic lesions (24), complicates this issue. Furthermore, Sanelli et al (25) have reported that TDP is not a major ubiquitinated target within the pathological inclusions of ALS.

From the Department of Neurology, Osaka University Graduate School of Medicine (HS, ME, SS), Yamadaoka, Suita; Department of Neuropathology, Institute of Neurological Sciences, Faculty of Medicine, Tottori University (SK), Nishi-cho, Yonago; Department of Health Science, Osaka University Graduate School of Medicine (YM), Yamadaoka, Suita; and Department of Neurology, Toneyama National Hospital (HF), Toneyama, Toyonaka, Japan.

Send correspondence and reprint requests to: Hisae Sumi, MD, PhD, Department of Neurology, Osaka University Graduate School of Medicine, 2-2 Yamadaoka, Suita, 565-0871, Japan; E-mail: hasumi@neurol.med.osaka-u.ac.jp

This study was supported by the Health and Labor Sciences Research on Measures for Incurable Disease, Ministry on Health, Labor and Welfare of Japan.

**TABLE.** Clinical and Pathological Data*

| Patients | Age, years | Disease Duration, years | Initial Weakness Manifestation | Use of Respirator (Estimated Duration) | Cause of Death | Family History | No. Large Neurons† | No. Large Neurons With TDP Mislocalization† | No. Neuronal Inclusions† | No. Glial Inclusions† |
|---|---|---|---|---|---|---|---|---|---|---|
| SALS r-1 | 69 | 0.7 | L | No | Pneumonia | No | 13 | 6 (I) | 40 | 16 |
| SALS r-2 | 77 | 0.8 | U | No | Resp. f. | No | 23 | 8 (I>D) | 34 | 4 |
| SALS r-3 | 49 | 0.8 | L, B | No | Resp. f. | No | 9 | 4 (I) | 35 | 6 |
| SALS r-4 | 60 | 1.5 | B, U | No | Pneumonia | No | 36 | 12 (D>I) | 25 | 38 |
| SALS r-5 | 59 | 1.5 | U | No | Resp. f. | No | 16 | 9 (D>I) | 12 | 22 |
| SALS r-6 | 69 | 2 | B, U | No | Resp. f. | No | 22 | 12 (D>I) | 25 | 38 |
| SALS r-7 | 51 | 2 | B | No | Resp. f. | No | 22 | 11 (D>I) | 21 | 11 |
| SALS r-8 | 71 | 2 | U | No | Resp. f. | No | 21 | 4 (I>D) | 69 | 8 |
| SALS r-9 | 61 | 2 | U | No | Resp. f. | No | 8 | 3 (I>D) | 12 | 9 |
| SALS r-10 | 64 | 2 | L | No | Pneumonia | No | 7 | 0 | 9 | 123 |
| SALS r-11 | 73 | 2.5 | B | No | Resp. f. | No | 25 | 4 (I>D) | 14 | 7 |
| SALS r-12 | 60 | 2.5 | B, U | No | Resp. f. | No | 12 | 7 (D>I) | 18 | 19 |
| SALS r-13 | 71 | 2.5 | U | No | Resp. f. | No | 4 | 0 | 26 | 26 |
| SALS s-1 | 79 | 5 | U | No | Resp. f. | No | 2 | 0 | 0 | 0 |
| SALS s-2 | 53 | 5.5 | U | No | Resp. f. | No | 9 | 0 | 4 | 2 |
| SALS s-3 | 63 | 5.5 | U, L | No | Resp. f. | No | 4 | 0 | 2 | 2 |
| SALS s-4 | 48 | 6.7 | ? | No | Resp. f. | No | 15 | 0 | 0 | 2 |
| SALS s-5 | 45 | 7.3 | ? | No | Resp. f. | No | 2 | 0 | 0 | 3 |
| | | | | Median (range), 62 (45–79); 2.0 (0.7–7.3) | | | | | | |
| ALS1-1 (C111Y) | 71 | 7 | L | 3 years | Ren f. | Yes | 0 | 0 | 20 | 31 |
| ALS1-2 (126 2bp del) | 42 | 2 | L | 0.5 years | Pneumonia | Yes | 3 | 1 (D) | 0 | 0 |
| ALS1-3 (126 2bp del) | 65 | 11 | L | 10 years | Hemorrhage | Yes | 0 | 0 | 0 | 0 |
| ALS1-4 (G37R) | 50 | 9 | U | 2.5 years | Pneumonia | Yes | 1 | 0 | 0 | 0 |
| ALS1-5 (L126S) | 67 | 9 | L | No | Resp. f. | Yes | 13 | 0 | 0 | 0 |
| ALS1-6 (L126S) | 45 | 8.5 | L | No | Resp. f. | Yes | 7 | 0 | 0 | 0 |
| | | | | Median (range), 58 (42–71); 9 (2–11) | | | | | | |

*ALS1, amyotrophic lateral sclerosis (*SOD-1* gene mutation); B, bulbar; D, diffuse staining pattern; D > I, predominantly diffuse staining pattern; I, inclusion pattern; I > D, predominantly inclusion pattern; L, lower limb; Ren. f., renal failure; Resp. f., respiratory failure; SALS r, sporadic ALS with a rapid clinical course (i.e. ≤2.5 years); SALS s, SALS with a slow clinical course; U, upper limb.

†Large neurons with cytoplasm exceeding 37 μm in diameter and clear nucleoli were counted. TAR DNA binding protein (TDP) mislocalization includes a diffuse staining pattern in the cytoplasm (D) and TDP-positive inclusions in the cytoplasm (I). Cell types containing TDP-positive inclusions were estimated as neuronal or glial on the basis of the morphology of their nuclei and cytoplasm.

To clarify how TDP may be involved in pathogenetic mechanisms in ALS, we examined SALS and ALS1 patients clinically and pathologically by immunohistochemistry using an anti-TDP antibody. We also examined the lumbar spinal cords of mutant SOD1 transgenic mice (G93A mice) that have lower copy numbers of the mutant *SOD1* gene than the G93A mice previously examined by Robertson et al (26); G93A mice with low copy numbers of the mutant *SOD1* gene show pathological changes that are similar to those in patients with ALS (27).

## MATERIALS AND METHODS

### ALS Cases and Pathological Assessment

Fixed paraffin-embedded 4-μm-thick sections through the lumbar spinal cord at the L5 level were obtained from Osaka University Graduate School of Medicine (Suita) for clinicopathologic analysis. These patients had SALS (n = 18; age at death 62 [median, 45–79] years; disease duration, 2 [0.7–7.3] years) or ALS1 (n = 6; age at death, 58 [42–71] years; disease duration, 9 [2–11] years; Table). All neuropathologic analyses were performed by trained neuropathologists. Sporadic ALS patients who did and did not have a history of respirator use and whose deaths were caused by respiratory failure or pneumonia were examined. Clinical data including the localization of initial symptoms, history of respirator use, cause of death, and family history are shown in the Table.

Deparaffinized sections were incubated for 30 minutes with 0.3% hydrogen peroxide to quench endogenous peroxidase activity and then washed with PBS. The primary antibodies used were rabbit polyclonal antibodies against TDP-43 (1:3000, Protein Tech Group, Chicago, IL) and ubiquitin (1:2000, Dako, Glostrup, Denmark), mouse monoclonal antibodies against human SOD1 (0.5 μg/mL, clone 1G2, MBL, Aichi, Japan) and phosphorylated neurofilament (1:10,000, SMI31, Covance, Berkeley, CA), and a sheep polyclonal antibody against human SOD1 (1:20,000, Calbiochem, San Diego, CA); these were applied to serial sections as primary antibodies. Goat anti-rabbit and anti-mouse immunoglobulins conjugated to peroxidase-labeled dextran polymer (ready to use, Dako Envision+, Dako Corp, Carpinteria, CA) and rabbit anti-sheep immunoglobulin (1:1000, Abcam PLC, Cambridge, United Kingdom) were used as secondary antibodies. Reaction products were visualized with 3,3′-diaminobenzidine tetrahydrochloride (ImmPACT DAB, Vector Laboratories, Burlingame, CA), and hematoxylin was used to counterstain cell nuclei.

To estimate the numbers of TDP-positive cytoplasmic inclusions, large neurons that had clear nucleoli and cell bodies with a diameter greater than 37 μm (28) (presumed to be α motoneurons) and the numbers of neurons with TDP mislocalization from the nucleus to the cytoplasm in the gray matter, from video images of each section obtained with a digital camera (Keyence VB-7010, Keyence, Osaka) attached to a light microscope (EclipseE800, Nikon, Tokyo), were counted. The diameters of the neurons were measured with the aid of image analysis software (VH-H1A5, Keyence). Mislocalization of TDP was defined as the presence of a TDP-negative nucleus and TDP-positive cytoplasm. In mislocalizations of TDP, there can also be diffuse staining patterns in the cytoplasm and TDP-positive filamentous or round inclusions in the cytoplasm. Cells containing TDP-positive inclusions were classified as neurons or glia on the basis of the shape of their nuclei and cytoplasm.

### Animals

Transgenic mice expressing the mutated human *SOD1* (G93A) gene at a low level (B6SJL-TgN[SOD1]-G93A)1Gur$^{dl}$ [G1L]) were obtained from Jackson Laboratory (Bar Harbor, ME). These mice carry 18 transgene copies because of a reduction in the copy number compared with (B6SJL-TgN[SOD1]-G93A)1Gur (G1H) mice, which express 25 copies (3). The G1L mice were bred and maintained as hemizygotes by mating with wild-type B6.SJL mice. Non-transgenic littermates were used as controls. All animals were genotyped and handled as previously described (29). We examined control (n = 6,292 [median, 240–296] days old) and G1L (n = 9,256 [224–281] days old, end stage) mice. One G1H mouse (120 days, end stage), also obtained from Jackson Laboratory, was examined to confirm the lack of TDP-43 abnormalities reported previously (26). *End stage* was defined as occurring when the mouse was so severely paralyzed that it could hardly move or drink water. The mice were killed with an overdose of sodium pentobarbital and perfused with PBS followed by 4% paraformaldehyde. The lumbar enlargement of the spinal cord was removed, immersed in 4% paraformaldehyde overnight at 4°C, and then dehydrated and embedded in paraffin blocks. Paraffin sections, 4-μm-thick, were prepared and stained with hematoxylin and eosin. Every fifth section (cut at 20-μm intervals) was obtained, and 4 sections from each mouse were used to count the total number of LBHIs in the sections. For immunohistochemistry, the primary antibodies used on the serial sections were against TDP-43 (1:600, Protein Tech Group) and human SOD1 (0.5 μg/mL, clone 1G2, MBL, Nagoya, Japan).

### Semiquantitative Analysis of Immunoreactivity for TDP

Because variation in the TDP immunoreactivity (TDP-IR) was evident among G1L mice, the patterns of TDP immunostaining were divided into normal (0) and abnormal (1 to 4), the latter showing TDP-positive neurites and inclusions and varying degrees of nuclear positivity. The stages of normal or abnormal patterns were classified by TDP-IR of the neuron nuclei as follows: normal pattern (Stage 0): same as in normal littermates, with immunoreactivity apparent only in nuclei; abnormal pattern (Stages 1–4): Stage 1, weak immunoreactivity in nuclei; Stage 2, weak to moderate immunoreactivity in nuclei; Stage 3, moderate to strong immunoreactivity in nuclei; Stage 4, strong immunoreactivity in nuclei.

### Quantitative Analysis of LBHIs

The numbers of LBHIs with a core and halo in neurons of the lumbar spinal cord were counted in hematoxylin and

eosin–stained sections (100× objective) from each G1L mouse as previously described (29).

## Statistical Analysis

Differences in the numbers of TDP-positive inclusions in neurons and glia and in large neurons (>37 μm) between SALS patients with a rapid course and those with a slow course were analyzed by Wilcoxon rank sum test. The relationships among the numbers of large neurons and TDP-positive inclusions in neurons and glia were also analyzed using Spearman correlation coefficient with a 95% confidence interval (CI). In G1L mice, the relationships among age at the end stage, number of LBHIs, and TDP-IR were analyzed using Spearman correlation coefficient with 95% CI. Exploratory subgroup analyses for age at the end stage were done in the TDP-IR weak groups (Stages 1 and 2) and the TDP-IR strong groups (Stages 3 and 4) by Kolmogorov-Smirnov test. All statistical analyses were performed with SAS version 9.1 (SAS Institute Inc, Cary, NC).

# RESULTS

## ALS Cases

In the lumbar cords of SALS patients with disease durations less than or equal to 2.5 years (SALS r-1 to -13), mislocalization of TDP was frequently observed (Figs. 1B, C; Table); this was not evident in controls (Fig. 1A). There was a diffuse cytoplasmic staining pattern, especially in large neurons (>37 μm, Fig. 1B) and TDP-positive filamentous or round inclusions were evident in atrophic neurons and in glia (Figs. 1C, D); the nuclei in the neurons and glia were negative for TDP. In SALS patients with mild to moderate neuronal loss, there was often a diffuse TDP staining pattern in the cytoplasm of large neurons (Table). No extracellular TDP-positive inclusions were apparent. By contrast, in SALS patients with disease durations longer than 5 years (SALS s-1 to -5), neurons with diffuse cytoplasmic staining patterns were not evident, and TDP-positive inclusions were only rarely detected (Table). The TDP-IR of the nuclei of residual neurons appeared to be preserved.

In ALS1 patients, diffuse cytoplasmic TDP staining of large neurons was found only in 1 patient, i.e. ALS1-2 (126 2bp del), who had a clinical course of 2 years (Table). Some small neurons in Patients ALS1-2 and ALS1-3 (126 2bp del) also showed diffuse cytoplasmic TDP staining (Figs. 3A, C). The TDP-positive inclusions were prominent in the glia and in small neurons or their neurites in Patient ALS1-1 (C111Y), who had no remaining large neurons. The nuclei of cells with TDP-positive inclusions were TDP negative (Figs. 2A, E). Colocalization of TDP and SOD1 was frequently evident as

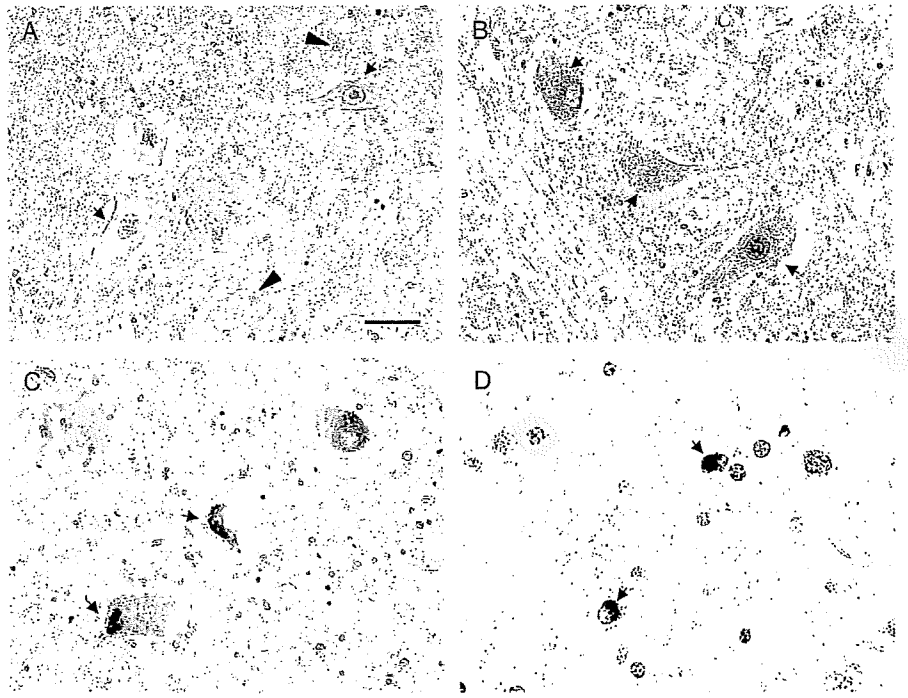


**FIGURE 1.** Mislocalization of TAR DNA binding protein (TDP) in cases of sporadic amyotrophic lateral sclerosis (SALS) with rapid clinical courses. **(A)** Normal control. The nuclei of large neurons are positive for TDP (arrows). Some glia (arrowheads) are weakly stained. **(B–D)** SALS patients. **(B)** There is diffuse punctate cytoplasmic staining in the neuron on the left (arrow), and heterogeneous staining in the middle (arrow) is observed in the cytoplasm. Nuclei of neurons on the left and in the middle are negative for TDP, whereas the nucleus of the neuron on the right is stained. **(C)** Variable appearances of cytoplasmic TDP inclusions (arrows). The structure on the left (arrow) is rounded, whereas the one in the middle neuron is elongated and filamentous (arrow). **(D)** Glial inclusions are positive for TDP (arrows). Immunohistochemistry against TDP. Scale bar = 50 μm.